UB-HET-09-02
May 2009

Measuring the Higgs Boson Self-coupling at High Energy e^+e^- Colliders

U. Baur*

Department of Physics, State University of New York,

Buffalo, NY 14260, USA

Abstract

Standard Model Higgs pair production at e^+e^- colliders has the capability to determine the Higgs boson self-coupling λ. I present a detailed analysis of the $e^+e^- \to ZHH$ and $e^+e^- \to \nu\bar{\nu}HH$ signal channels, and the relevant background processes, for future e^+e^- linear colliders with center of mass energies of $\sqrt{s} = 0.5$ TeV, 1 TeV, and 3 TeV. Special attention is given to the role non-resonant Feynman diagrams play, and the theoretical uncertainties of signal and background cross sections. I also derive quantitative sensitivity limits for λ. I find that an e^+e^- collider with $\sqrt{s} = 0.5$ TeV can place meaningful bounds on λ only if the Higgs boson mass is relatively close to its current lower limit. At an e^+e^- collider with $\sqrt{s} = 1$ TeV (3 TeV), λ can be determined with a precision of $20 - 80\%$ ($10 - 20\%$) for integrated luminosities in the few ab^{-1} range and Higgs boson masses in the range $m_H = 120 - 180$ GeV.

*baur@ubhex.physics.buffalo.edu

I. INTRODUCTION

The CERN Large Hadron Collider (LHC) is scheduled to begin operation in 2009, beginning a new era wherein the mechanism of electroweak symmetry breaking and fermion mass generation will be revealed and studied in detail. Although alternative mechanisms exist in theory, this is generally believed to be a light Higgs boson with mass 114 GeV $< m_H <$ 145 GeV [1–3]. More specifically, we expect a fundamental scalar sector which undergoes spontaneous symmetry breaking as the result of a potential which acquires a nonzero vacuum expectation value. The LHC will easily find a light Standard Model (SM) Higgs boson with moderate luminosity [4,5]. Moreover, the LHC will have the capability to determine some of its properties [6,7], such as its fermionic and bosonic decay modes and couplings [8–11], including invisible decays [12] and possibly even rare decays to second generation fermions [13]. An e^+e^- linear collider with a center of mass energy of 350 GeV or more will be able to significantly improve these preliminary measurements, in some cases by an order of magnitude in precision, if an integrated luminosity of 500 fb^{-1} can be achieved [14].

Perhaps the most important measurement after a Higgs boson discovery is of the Higgs potential itself, which requires measurement of the trilinear and quartic Higgs boson self-couplings. Only multiple Higgs boson production can probe these directly [15–17]. Several years ago, studies exploring the potential of the LHC, a luminosity-upgraded LHC (SLHC) with roughly ten times the amount of data expected in the first run, and a Very Large Hadron Collider (VLHC), have appeared in the literature [18–22]. There are also numerous quantitative sensitivity limit analyses of Higgs boson pair production in e^+e^- collisions ranging from 500 GeV to 3 TeV center of mass energies [16,17,23–30], and for $\gamma\gamma \to HH$ [31]. The e^+e^- studies, usually, focus on one particular Higgs mass and/or final state, only one center of mass energy, and, in many cases, estimate the background using a leading-log shower approximation. Furthermore, the effects of non-resonant Feynman diagrams are not taken into account.

In this paper, I present a more thorough investigation of Higgs boson pair production in e^+e^- collisions. I calculate the $e^+e^- \to ZHH$ and $e^+e^- \to \nu\bar{\nu}HH$ ($\nu = \nu_e, \nu_\mu, \nu_\tau$) signal cross sections for $\sqrt{s} = 0.5$ TeV, 1 TeV and 3 TeV, and $m_H = 120$ GeV, 140 GeV and 180 GeV, although $m_H = 180$ GeV is disfavored by the most recent fit to electroweak data when direct search limits from the Tevatron experiments are taken into account [3]. A center of mass energy of $0.5 - 1$ TeV is considered for the International Linear Collider (ILC) [32], whereas $\sqrt{s} = 3$ TeV is the target energy for CERN's CLIC concept [33]. Only unpolarized electron and positron beams are considered. Since the cross section for the one-loop process $e^+e^- \to HH$ is more than one order of magnitude smaller than that for ZHH production [34], it is not considered here. Likewise, I will ignore the process $e^+e^- \to e^+e^-HH$; due to the small Zee coupling, its cross section is about a factor 6 less than that for $\nu\bar{\nu}HH$ production [35]. I consider several final states, and estimate both the reducible and irreducible backgrounds using exact matrix element calculations. Special attention is given to the role non-resonant Feynman diagrams play, and the theoretical uncertainties of signal and background cross sections. All calculations are performed taking into account the anticipated resolution of future e^+e^- detectors. Finally, I derive quantitative sensitivity bounds for several integrated luminosities, and compare the capabilities of the

considered e^+e^- colliders with each other and those of the LHC, a luminosity upgraded LHC (SLHC) [18], and a Very Large Hadron Collider operating at a center of mass energy of 200 TeV [36].

The remainder of this paper is organized as follows. I first review the definition of the Higgs boson self-couplings and briefly discuss SM and non-SM predictions for these parameters in Sec. II. The methods and tools used in my calculations, together with the parametrized detector resolution are summarized in Sec. III. In Secs. IV and V the ZHH and $\nu\bar{\nu}HH$ signal channels and all relevant backgrounds are discussed. Quantitative sensitivity limits are calculated in Sec. VI. In Sec. VII, I finally present my conclusions.

II. HIGGS BOSON SELF-COUPLINGS

The trilinear and quartic Higgs boson couplings λ and $\tilde{\lambda}$ are defined through the potential

$$V(\eta_H) \,=\, \frac{1}{2}\, m_H^2\, \eta_H^2 \,+\, \lambda\, v\, \eta_H^3 \,+\, \frac{1}{4}\, \tilde{\lambda}\, \eta_H^4, \tag{1}$$

where η_H is the physical Higgs field, $v = (\sqrt{2}G_F)^{-1/2}$ is the vacuum expectation value, and G_F is the Fermi constant. In the SM the self-couplings are

$$\tilde{\lambda} = \lambda = \lambda_{SM} = \frac{m_H^2}{2v^2}\,. \tag{2}$$

Regarding the SM as an effective theory, the Higgs boson self-couplings λ and $\tilde{\lambda}$ are *per se* free parameters, and S-matrix unitarity constrains $\tilde{\lambda}$ to $\tilde{\lambda} \leq 8\pi/3$ [37]. Since future collider experiments likely cannot probe $\tilde{\lambda}$ [38], I concentrate on the trilinear coupling λ in the following. The quartic Higgs coupling does not affect the Higgs pair production processes I consider.

In the SM, radiative corrections decrease λ by $4-11\%$ for $120\ \text{GeV} < m_H < 200\ \text{GeV}$ [39]. Larger deviations are possible in scenarios beyond the SM. For example, in two Higgs doublet models where the lightest Higgs boson is forced to have SM like couplings to vector bosons, quantum corrections may increase the trilinear Higgs boson coupling by up to 100% [39]. In the MSSM, loop corrections modify the self-coupling of the lightest Higgs boson in the decoupling limit, which has SM-like couplings, by up to 8% for light stop squarks [40]. Anomalous Higgs boson self-couplings also appear in various other scenarios beyond the SM, such as models with a composite Higgs boson [41], or in Little Higgs models [42]. In many cases, the anomalous Higgs boson self-couplings can be parametrized in terms of higher dimensional operators which are induced by integrating out heavy degrees of freedom. A systematic analysis of Higgs boson self-couplings in a higher dimensional operator approach can be found in Ref. [43].

III. CALCULATIONAL DETAILS

All calculations presented here have been performed at tree-level using `MadEvent` [44] which has been modified to allow for non-standard values of λ. For some background calculations it was also necessary to increase the maximum number of Feynman diagrams and/or

configurations allowed so that `MadEvent` could be used successfully. Background calculations involving the strong coupling constant, α_s, were performed with the renormalization scale set to $\mu = M_Z$, where M_Z is the mass of the Z-boson. The SM parameters used are [45]

$$G_\mu = 1.16639 \times 10^{-5}\ \text{GeV}^{-2}, \tag{3}$$

$$M_Z = 91.188\ \text{GeV}, \quad M_W = 80.419\ \text{GeV}, \tag{4}$$

$$\sin^2\theta_W = 1 - \left(\frac{M_W^2}{M_Z^2}\right), \quad \alpha_{G_\mu} = \frac{\sqrt{2}}{\pi}\, G_F \sin^2\theta_W M_W^2, \tag{5}$$

where G_F is the Fermi constant, M_W is the W mass, θ_W is the weak mixing angle, and α_{G_μ} is the electromagnetic coupling constant in the G_μ scheme.

The basic kinematic acceptance cuts for events at the ILC and CLIC are

$$\begin{aligned} &E_\ell > 15\ \text{GeV}, \qquad E_j > 15\ \text{GeV}, \qquad \not{p}_T > 15\ \text{GeV}, \\ &5^\circ < \theta(j, \text{beam}) < 175^\circ\,, \qquad \theta(j, j') > 10^\circ, \\ &5^\circ < \theta(\ell, \text{beam}) < 175^\circ\,, \qquad \theta(\ell, j) > 10^\circ, \end{aligned} \tag{6}$$

where $\theta(k, l)$ is the angle between the two objects k and l, $\ell = e$, μ, E is the energy, and $\not{p}_T$ is the missing transverse momentum. The $\not{p}_T$ cut is only imposed on final states where there are one or more neutrinos present. Likewise, the angular and energy cuts on the charged leptons are only imposed if there is at least one charged lepton in the event which does not result from the decay of a charm or bottom quark.

In all calculations, I include minimal detector effects by Gaussian smearing of the parton momenta according to ILC detector expectations [46]

$$\begin{aligned} \frac{\Delta E}{E}(\text{had}) &= \frac{0.405}{\sqrt{E}}, \\ \frac{\Delta E}{E}(\text{lep}) &= \frac{0.102}{\sqrt{E}}, \end{aligned} \tag{7}$$

and assume that charged leptons and jets can be detected with an efficiency close to 100%. For the b-tagging efficiency, ϵ_b, and the associated misidentification probabilities of light quark/gluon jets and c-quarks to be tagged as a b-quarks, $P_{j\to b}$ and $P_{c\to b}$, I consider two scenarios [47,48]:

$$\epsilon_b = 90\% \text{ with } P_{j\to b} = 0.5\% \text{ and } P_{c\to b} = 10\%, \tag{8}$$

and

$$\epsilon_b = 80\% \text{ with } P_{j\to b} = 0.1\% \text{ and } P_{c\to b} = 2\%. \tag{9}$$

The energy loss in b-jets due to b-quark decays is taken into account via a parametrized function [49], and I will assume that b- and $\bar{b}$-quarks can be distinguished with 100% efficiency. This should be a good approximation since ILC detectors are expected to be able to measure the electric charge of a b-jet with an efficiency of 90% or better [48,50].

The identification of $H \to b\bar{b}$ and hadronic W- and Z-decays plays an important role in separating the ZHH and $\nu\bar{\nu}HH$ signal from the background. To identify $W \to jj$ and $Z \to jj$ decays, I require ($V = W$, Z)

$$|M_V - m(jj)| < 8 \text{ GeV}, \tag{10}$$

where $m(jj)$ is the di-jet invariant mass. Since the energy loss of the b-jets distorts the $H \to b\bar{b}$ Breit-Wigner function and lowers the $b\bar{b}$ invariant mass, I impose

$$100 \text{ GeV} < m(b\bar{b}) < 126 \text{ GeV} \qquad \text{for } m_H = 120 \text{ GeV and,} \tag{11}$$
$$120 \text{ GeV} < m(b\bar{b}) < 150 \text{ GeV} \qquad \text{for } m_H = 140 \text{ GeV.} \tag{12}$$

This captures most of the signal cross section. I also assume that, by the time Higgs pair production is being analyzed, the Higgs boson mass is accurately known from experiments at the LHC and/or an analysis of the process $e^+e^- \to ZH$. Initial state radiation and beamstrahlung are not included in any of the calculations presented here.

In order to derive sensitivity limits for λ, the distribution of Higgs-pair invariant mass, M_{HH}, will be used. The M_{HH} distribution is known to be sensitive to the Higgs boson self-coupling, in particular for small values of the Higgs-pair mass [25].

It is well known [16,23] that the $e^+e^- \to ZHH$ cross section decreases with increasing center of mass energy while $\sigma(e^+e^- \to \nu\bar{\nu}HH)$ increases. For $\sqrt{s} = 0.5$ TeV, $\sigma(e^+e^- \to ZHH) \gg \sigma(e^+e^- \to \nu\bar{\nu}HH)$, and for $\sqrt{s} = 3$ TeV, $\sigma(e^+e^- \to ZHH) \ll \sigma(e^+e^- \to \nu\bar{\nu}HH)$. For $\sqrt{s} = 1$ TeV, the two cross sections are of the same order of magnitude, with $e^+e^- \to \nu\bar{\nu}HH$ being the larger source of Higgs boson pairs. I, therefore, consider ZHH ($\nu\bar{\nu}HH$) production for $\sqrt{s} \leq 1$ TeV ($\sqrt{s} \geq 1$ TeV) only. For a center of mass energy of 0.5 TeV, Higgs pair production is strongly phase space suppressed if $m_H > 140$ GeV [21]. The $m_H = 180$ GeV case, therefore, is only analyzed for $\sqrt{s} \geq 1$ TeV.

As stated before, all calculations reported here are carried out at tree level. The complete one-loop radiative corrections to $e^+e^- \to ZHH$ and $e^+e^- \to \nu\bar{\nu}HH$ are known [51,52] to modify the lowest cross section by a few percent for the energy range considered in this paper. As I will show, for most of the final states considered in this paper, there are uncertainties which are significantly larger than the effect of the one-loop electroweak radiative corrections. Electroweak radiative corrections thus will be ignored in the following.

IV. ZHH ANALYSIS

The total $e^+e^- \to ZHH$ cross section at $\sqrt{s} = 0.5$ TeV is $\sigma(ZHH) \approx 0.18$ fb. It decreases with increasing center of mass energy and Higgs boson mass. The current design luminosity of the ILC is [32] $\mathcal{L} = 2 \times 10^{34}\,\text{cm}^{-2}\text{s}^{-1}$, corresponding to a yearly integrated luminosity of 200 fb^{-1}. One therefore expects a total of about 40 ZHH events per year at such a machine, before Z- and Higgs boson decays, and experimental acceptance cuts and efficiencies, are taken into account.

With an expected b-tagging efficiency of 80% or higher, and a fairly large branching ratio ($B(H \to b\bar{b}) \approx 68\%$ (33%) for $m_H = 120$ GeV ($m_H = 140$ GeV)), requiring $HH \to b\bar{b}b\bar{b}$ and $Z \to \ell^+\ell^-$ ($\ell = e, \mu$) offers the best chance to identify ZHH events. Unfortunately, the $Z \to \ell^+\ell^-$ branching ratio is very small, and too few $\ell^+\ell^- b\bar{b}b\bar{b}$ events are left to make this final state viable for a measurement of the Higgs boson self-coupling. I therefore concentrate on the $ZHH \to jjb\bar{b}b\bar{b}$ final state, where jj denotes a light jet pair consistent with originating from a Z-boson (i.e. satisfying Eq. (10)) and which is not tagged as a b-pair. This explicitly

removes $Z \to b\bar{b}$ decays, reducing the combinatorial background and simplifying the analysis. Since additional jets tend to weaken the sensitivity limits for λ [53], I require exactly two light jets, and four tagged b-quarks in events. Two or more pairs of b-quarks have to satisfy Eq. (11) or (12).

In addition to the four Feynman diagrams contributing to the $\mathcal{O}(\alpha^3)$ $e^+e^- \to ZHH \to jjb\bar{b}b\bar{b}$ signal, there are approximately 8,500 $\mathcal{O}(\alpha^6)$, $\mathcal{O}(\alpha_s^4\alpha^2)$ and $\mathcal{O}(\alpha_s^2\alpha^4)$ non-resonant and single Higgs resonant diagrams contributing to the same final state. Single-resonant Higgs and the $\mathcal{O}(\alpha_s^4\alpha^2)$ diagrams constitute the potentially largest background contributions. In Ref. [24], the role of the non-resonant and single resonant $\mathcal{O}(\alpha_s^2\alpha^2)$ and $\mathcal{O}(\alpha^4)$ diagrams in $e^+e^- \to ZHH \to Zb\bar{b}b\bar{b}$ was analyzed in the limit of a stable Z-boson. It was found that the contribution of the $\mathcal{O}(\alpha_s^2\alpha^2)$ diagrams was small compared with the signal for $m_H \leq 140$ GeV. However, the background from $\mathcal{O}(\alpha^4)$ single Higgs production can be substantial, in particular for $m_H > 130$ GeV. Misidentification of light jets and charm quarks also contribute to the background for $jjb\bar{b}b\bar{b}$ production.

Using the cuts and efficiencies listed in Eqs. (6) and (8), and requiring one light jet pair satisfying Eq. (10) and four tagged b-jets with at least two pairs fulfilling Eq. (11), I calculate the cross section of the $ZHH \to jjb\bar{b}b\bar{b}$ signal, the cross section for $e^+e^- \to jjb\bar{b}b\bar{b}$ including all $\mathcal{O}(\alpha^6)$, $\mathcal{O}(\alpha_s^4\alpha^2)$ and $\mathcal{O}(\alpha_s^2\alpha^4)$ diagrams, the $e^+e^- \to jjb\bar{b}c\bar{c}$ background (approximately 7,300 $\mathcal{O}(\alpha^6)$, $\mathcal{O}(\alpha_s^4\alpha^2)$ and $\mathcal{O}(\alpha_s^2\alpha^4)$ diagrams), the $b\bar{b}4j$ background (approximately 15,600 $\mathcal{O}(\alpha^6)$, $\mathcal{O}(\alpha_s^4\alpha^2)$ and $\mathcal{O}(\alpha_s^2\alpha^4)$ diagrams), and the $\mathcal{O}(\alpha_s^4\alpha^2)$ $e^+e^- \to 6j$ background (approximately 7,600 diagrams). The signal is calculated for the SM Higgs self-coupling ($\Delta\lambda_{HHH} = 0$), $\Delta\lambda_{HHH} = +1$, and $\Delta\lambda_{HHH} = -1$, where

$$\Delta\lambda_{HHH} = \lambda_{HHH} - 1 = \frac{\lambda}{\lambda_{SM}} - 1. \tag{13}$$

The results for the Higgs pair invariant mass distribution with $\sqrt{s} = 0.5$ TeV (1 TeV), and $m_H = 120$ GeV and $m_H = 140$ GeV are shown in Fig. 1 (Fig. 2). The solid black lines show the prediction for the SM $e^+e^- \to ZHH \to jjb\bar{b}b\bar{b}$ signal. Since it is impossible to know which b-quark has to be paired with which $\bar{b}$-quark when reconstructing the Higgs bosons in the event, there is a combinatorial background from incorrect pairing, which is largest close to threshold. The dashed histogram in Fig. 1a shows that the combinatorial background indeed dominates the signal cross section close to threshold, but dies out quickly for larger values of M_{HH}. Similar results are obtained for different Higgs boson masses and center of mass energies.

The dashed and dotted lines give the M_{HH} distribution for $\Delta\lambda_{HHH} = +1$ and $\Delta\lambda_{HHH} = -1$, respectively. They demonstrate that the Higgs pair invariant mass distribution is sensitive to the Higgs self-coupling λ, especially for small values of M_{HH}. Positive (negative) values of $\Delta\lambda_{HHH}$ increase (decrease) the ZHH cross section. The magenta curves give the SM cross section for $e^+e^- \to jjb\bar{b}b\bar{b}$ including the full set of $\mathcal{O}(\alpha^6)$, $\mathcal{O}(\alpha_s^4\alpha^2)$ and $\mathcal{O}(\alpha_s^2\alpha^4)$ Feynman diagrams. For $m_H = 120$ GeV and $\sqrt{s} = 0.5$ TeV and the renormalization scale set to $\mu = M_Z$, the contribution from the single-resonant and non-resonant electroweak and QCD diagrams, and the interference effects between these diagrams and the ZHH signal diagrams, decrease the cross section for $jjb\bar{b}b\bar{b}$ production by about 10%. For $m_H = 140$ GeV at the same center of mass energy, however, taking into account the single-resonant and non-resonant electroweak and QCD diagrams almost doubles the cross section. Since these

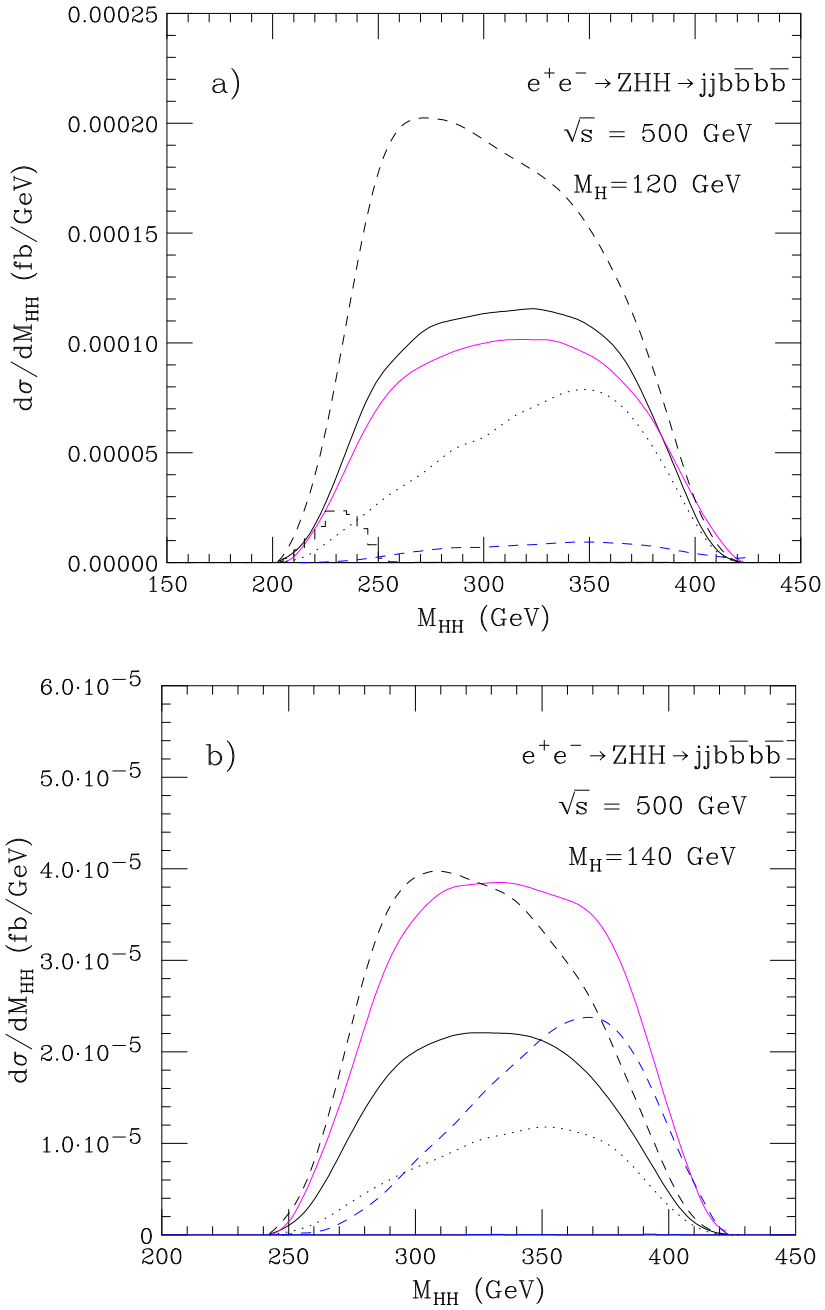

FIG. 1. The $e^+e^- \to ZHH \to jjb\bar{b}b\bar{b}$ cross section with four b-tags as a function of the Higgs pair invariant mass, M_{HH}, for $\sqrt{s} = 0.5$ TeV and a) $m_H = 120$ GeV and b) $m_H = 140$ GeV. The black solid line is the prediction of the SM signal cross section. The black dashed and dotted lines correspond to the ZHH signal cross section for $\Delta\lambda_{HHH} = +1$ and $\Delta\lambda_{HHH} = -1$, respectively. The dashed histogram in part a) represents the combinatorial background from incorrectly assigned $b\bar{b}$ pairs in the signal. The magenta line shows the SM cross section for $e^+e^- \to jjb\bar{b}b\bar{b}$ including the full set of $\mathcal{O}(\alpha^6)$, $\mathcal{O}(\alpha_s^4\alpha^2)$ and $\mathcal{O}(\alpha_s^2\alpha^4)$ Feynman diagrams. The dashed blue line corresponds to the $jjb\bar{b}c\bar{c}$ cross section. The cuts imposed and the efficiencies used are summarized in Eqs. (6), (8), and (10) – (12).

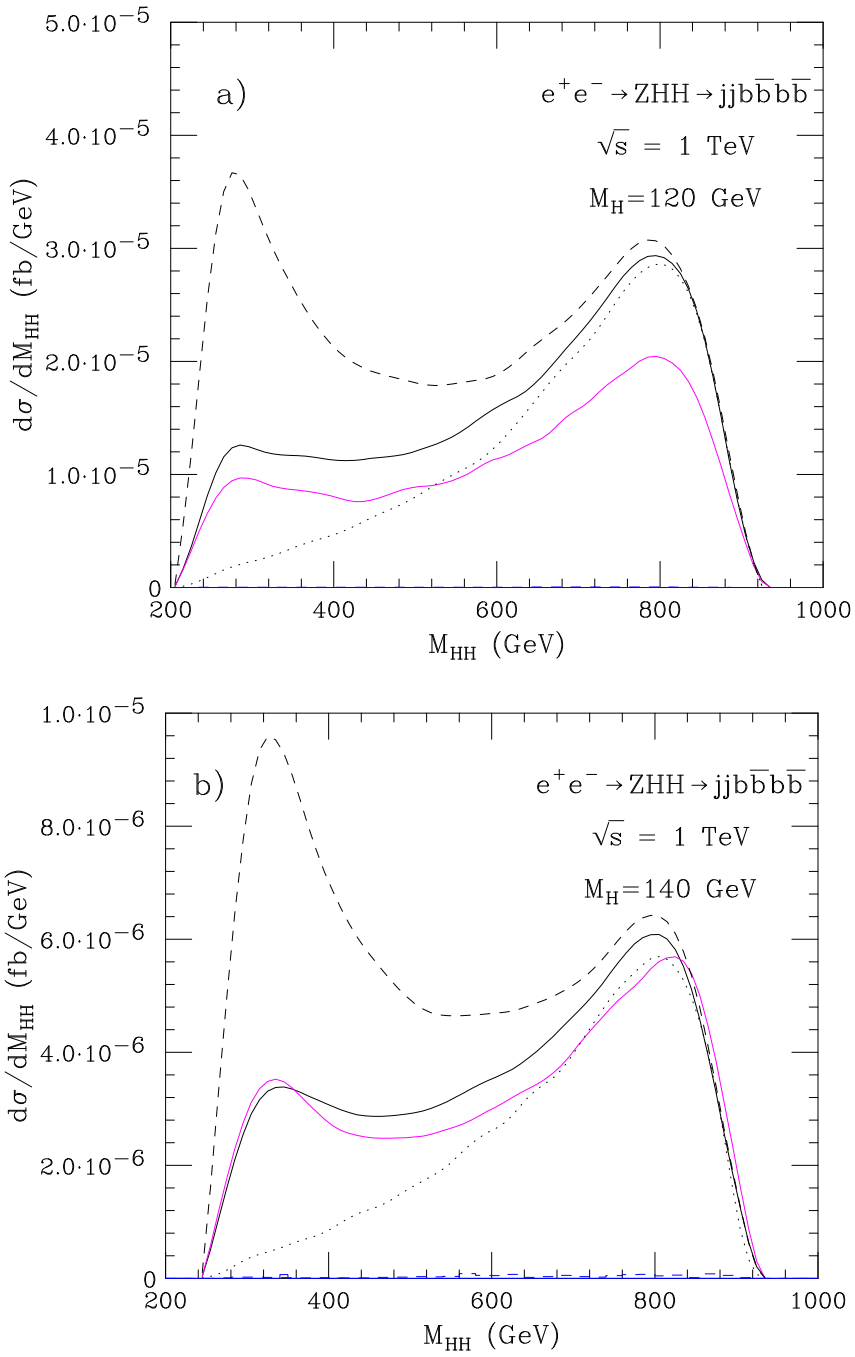

FIG. 2. The $e^+e^- \to ZHH \to jjb\bar{b}b\bar{b}$ cross section with four b-tags as a function of the Higgs pair invariant mass, M_{HH}, for $\sqrt{s} = 1$ TeV and a) $m_H = 120$ GeV and b) $m_H = 140$ GeV. The black solid line is the prediction of the SM signal cross section. The black dashed and dotted lines correspond to the ZHH signal cross section for $\Delta\lambda_{HHH} = +1$ and $\Delta\lambda_{HHH} = -1$, respectively. The magenta line shows the SM cross section for $e^+e^- \to jjb\bar{b}b\bar{b}$ including the full set of $\mathcal{O}(\alpha^6)$, $\mathcal{O}(\alpha_s^4\alpha^2)$ and $\mathcal{O}(\alpha_s^2\alpha^4)$ Feynman diagrams. The dashed blue line corresponds to the $jjb\bar{b}c\bar{c}$ cross section. The cuts imposed and the efficiencies used are summarized in Eqs. (6), (8), and (10) – (12).

diagrams do not depend on the Higgs self-coupling, this considerably reduces the sensitivity to λ for $m_H = 140$ GeV. Due to the reduced phase space and the smaller $H \to b\bar{b}$ branching ratio, the $ZHH \to jjb\bar{b}b\bar{b}$ cross section for $m_H = 140$ GeV is about a factor 8 smaller than that for $m_H = 120$ GeV. As I will show in Sec. VI, the reduction in signal cross section, combined with the increase of the single-resonant and non-resonant background, will make it very difficult to measure the Higgs self-coupling in $jjb\bar{b}b\bar{b}$ production for $m_H > 120$ GeV at an e^+e^- collider with $\sqrt{s} = 500$ GeV.

The contribution of the non-resonant diagrams to the $jjb\bar{b}b\bar{b}$ cross section can, in principle, be reduced by imposing a tighter cut on the $b\bar{b}$ invariant mass. However, the energy loss of b-quarks, combined with the finite resolution of detectors smears out the Higgs boson resonance over a fairly large $b\bar{b}$ invariant mass range. A more stringent $m(b\bar{b})$ cut thus would, at the same time, considerably reduce the signal cross section.

For $\sqrt{s} = 1$ TeV and $m_H = 120$ GeV ($m_H = 140$ GeV), the single-resonant and non-resonant background diagrams lower the cross section by up to 50% (20%). The cross section reduction is mainly caused by the interference of resonant $Z \to jj$, and non-resonant diagrams. Note that the effect of the single- and non-resonant background can easily be confused with that of a non-SM Higgs self-coupling, especially for a small number of signal events. At $\sqrt{s} = 1$ TeV, the reducible backgrounds are almost negligible. The SM cross section peaks in the region which is least sensitive to λ_{HHH}. Given a sufficient integrated luminosity, this makes it possible to use the high M_{HH} region to normalize the cross section. Unfortunately, this method does not work for $\sqrt{s} = 0.5$ TeV, where non-standard Higgs self-couplings lead to a broad enhancement or reduction of the cross section, spread out over most of the accessible M_{HH} range.

The largest reducible background to $ZHH \to jjb\bar{b}b\bar{b}$ originates from $jjb\bar{b}c\bar{c}$ production where both c-quarks are mistagged as b-jets. This background is only significant for $\sqrt{s} = 0.5$ TeV and $m_H = 140$ GeV. The $b\bar{b}4j$ background where two light jets are misidentified as b-jets, and the $e^+e^- \to 6j$ background where four jets are mistagged, are very small and are not shown in Figs. 1 and 2.

Although the expected b-tagging efficiency at the ILC is very high, requiring four tagged b-quarks reduces the observable cross section by a factor 0.66 for $\epsilon_b = 0.9$. Since the signal cross section is very small, it is natural to explore whether it is advantageous to reduce the number of required b-tagged jets. Reducing the number of required b-tags from four to three increases the signal cross section by a factor

$$1 + \frac{4(1-\epsilon_b)}{\epsilon_b} \tag{14}$$

ie. for $\epsilon_b = 0.9$ by about a factor 1.44. However, the $jjb\bar{b}c\bar{c}$ background increases by about a factor 10, while the $b\bar{b}4j$ and $6j$ backgrounds grow by more than two orders of magnitude. Furthermore, $b\bar{b}cjjj$ production now also contributes to the background. The M_{HH} distribution for $ZHH \to jjb\bar{b}b\bar{b}$ with three tagged b-quarks and $\sqrt{s} = 0.5$ TeV (1 TeV) is shown in Fig. 3 (Fig. 4). To calculate the cross sections shown in these figures, I require one light jet pair in the mass window given in Eq. (10), one tagged $b\bar{b}$ pair and at least one bj combination with an invariant mass satisfying Eq. (11) or (12). For a center of mass energy of 0.5 TeV, the $jjb\bar{b}c\bar{c}$ (dashed blue line or histogram), $b\bar{b}cjjj$ (solid blue line or histogram), and the $b\bar{b}4j$ background (solid red line or histogram) are all significantly larger than the

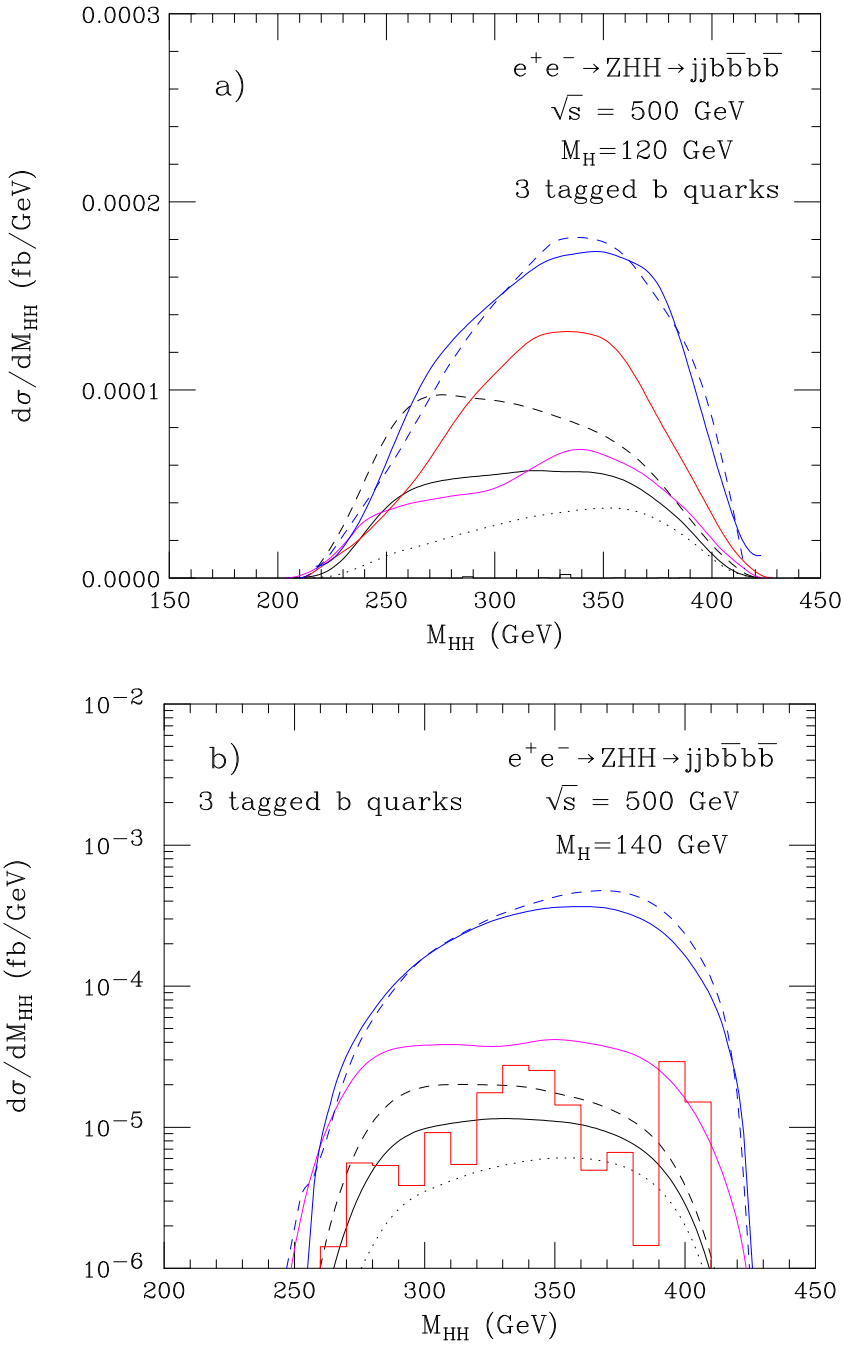

FIG. 3. The $e^+e^- \to ZHH \to jjb\bar{b}b\bar{b}$ cross section with three b-tags as a function of the Higgs pair invariant mass, M_{HH}, for $\sqrt{s} = 0.5$ TeV and a) $m_H = 120$ GeV and b) $m_H = 140$ GeV. The black solid line is the prediction of the SM signal cross section. The black dashed and dotted lines correspond to the ZHH signal cross section for $\Delta\lambda_{HHH} = +1$ and $\Delta\lambda_{HHH} = -1$, respectively. The magenta line shows the SM cross section for $e^+e^- \to jjb\bar{b}b\bar{b}$ including the full set of $\mathcal{O}(\alpha^6)$, $\mathcal{O}(\alpha_s^4\alpha^2)$ and $\mathcal{O}(\alpha_s^2\alpha^4)$ Feynman diagrams. The solid (dashed) blue and red lines or histograms correspond to the $b\bar{b}cjjj$ ($jjb\bar{b}c\bar{c}$) and $b\bar{b}4j$ cross section, respectively. The cuts imposed and the efficiencies used are summarized in Eqs. (6), (8), and (10) – (12).

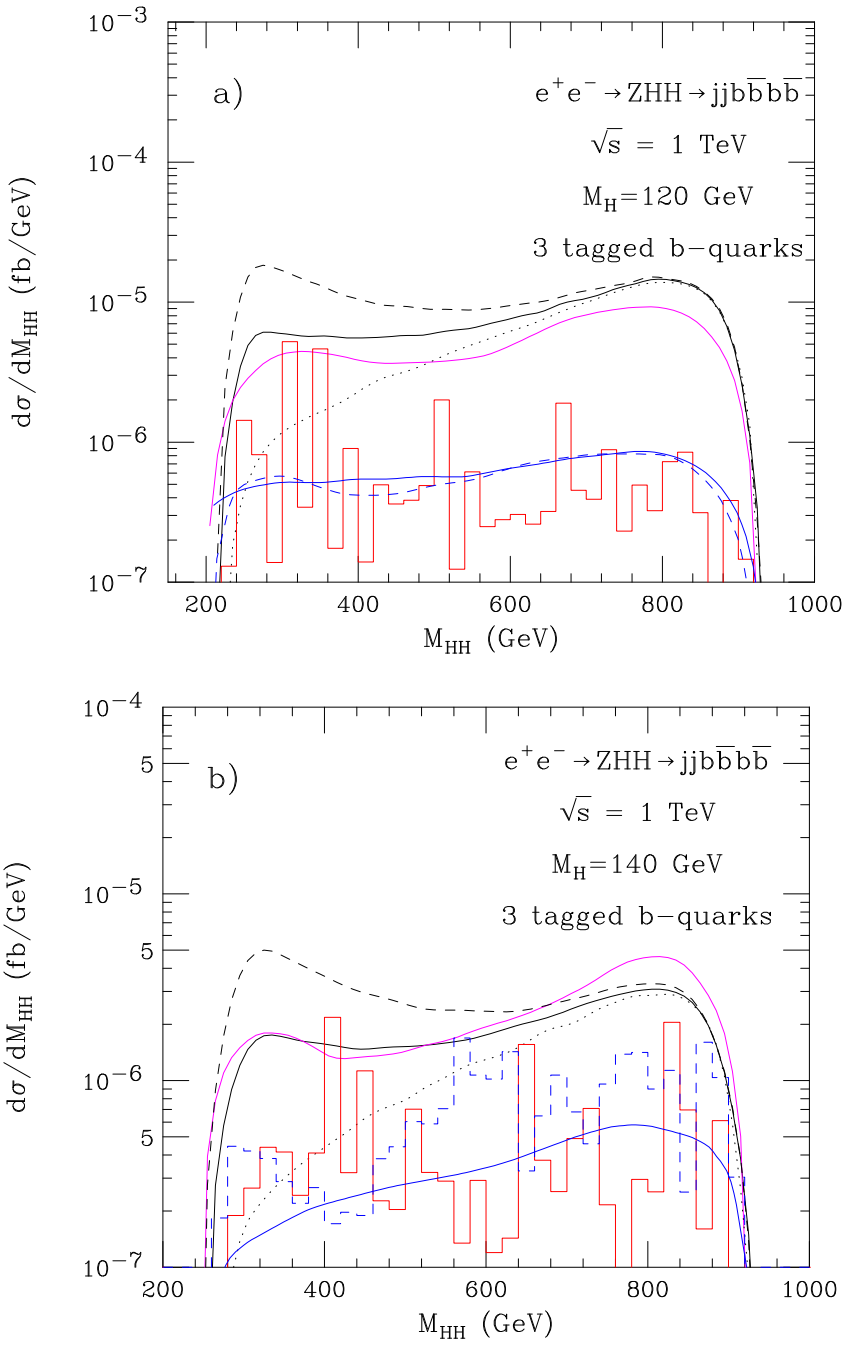

FIG. 4. The $e^+e^- \to ZHH \to jjb\bar{b}b\bar{b}$ cross section with three b-tags as a function of the Higgs pair invariant mass, M_{HH}, for $\sqrt{s} = 1$ TeV and a) $m_H = 120$ GeV and b) $m_H = 140$ GeV. The black solid line is the prediction of the SM signal cross section. The black dashed and dotted lines correspond to the ZHH signal cross section for $\Delta\lambda_{HHH} = +1$ and $\Delta\lambda_{HHH} = -1$, respectively. The magenta line shows the SM cross section for $e^+e^- \to jjb\bar{b}b\bar{b}$ including the full set of $\mathcal{O}(\alpha^6)$, $\mathcal{O}(\alpha_s^4\alpha^2)$ and $\mathcal{O}(\alpha_s^2\alpha^4)$ Feynman diagrams. The solid (dashed) blue and red lines or histograms correspond to the $b\bar{b}cjjj$ ($jjb\bar{b}c\bar{c}$) and $b\bar{b}4j$ cross section, respectively. The cuts imposed and the efficiencies used are summarized in Eqs. (6), (8), and (10) – (12).

TABLE I. Cross sections in fb for $e^+e^- \to jjb\bar{b}b\bar{b}$ for $m_H = 120$ GeV and $m_H = 140$ GeV, and $\sqrt{s} = 0.5$ TeV and $\sqrt{s} = 1$ TeV. Shown are the results for the SM signal, the full set of $\mathcal{O}(\alpha^6)$, $\mathcal{O}(\alpha_s^4\alpha^2)$ and $\mathcal{O}(\alpha_s^2\alpha^4)$ Feynman diagrams (labeled "all"), and the total reducible backgrounds (labeled "bgd"), with 3, 4 and ≥ 3 b-tags. Cross sections are listed for two sets of b-tagging efficiencies and light quark/gluon jet and charm quark misidentification probabilities (see Eqs. (8) and (9)).

$\epsilon_b = 0.9$, $P_{c\to b} = 0.1$, $P_{j\to b} = 0.005$									
	4 b-tags			3 b-tags			≥ 3 b-tags		
	signal	all	bgd	signal	all	bgd	signal	all	bgd
$\sqrt{s} = 0.5$ TeV, $m_H = 120$ GeV	0.016	0.014	0.001	0.008	0.008	0.061	0.024	0.022	0.062
$\sqrt{s} = 0.5$ TeV, $m_H = 140$ GeV	0.002	0.004	0.002	0.001	0.005	0.077	0.003	0.009	0.079
$\sqrt{s} = 1$ TeV, $m_H = 120$ GeV	0.011	0.008	$2 \cdot 10^{-5}$	0.005	0.004	0.001	0.016	0.013	0.001
$\sqrt{s} = 1$ TeV, $m_H = 140$ GeV	0.002	0.002	$2 \cdot 10^{-5}$	0.0012	0.0015	0.0010	0.003	0.004	0.001
$\epsilon_b = 0.8$, $P_{c\to b} = 0.02$, $P_{j\to b} = 0.001$									
	4 b-tags			3 b-tags			≥ 3 b-tags		
	signal	all	bgd	signal	all	bgd	signal	all	bgd
$\sqrt{s} = 0.5$ TeV, $m_H = 120$ GeV	0.010	0.009	$3 \cdot 10^{-5}$	0.011	0.011	0.010	0.021	0.020	0.010
$\sqrt{s} = 0.5$ TeV, $m_H = 140$ GeV	0.001	0.002	$6 \cdot 10^{-5}$	0.001	0.007	0.012	0.002	0.009	0.012
$\sqrt{s} = 1$ TeV, $m_H = 120$ GeV	0.007	0.005	0	0.007	0.006	$2 \cdot 10^{-4}$	0.014	0.011	$2 \cdot 10^{-4}$
$\sqrt{s} = 1$ TeV, $m_H = 140$ GeV	0.001	0.001	0	0.0017	0.0021	$2 \cdot 10^{-4}$	0.003	0.003	$2 \cdot 10^{-4}$

ZHH signal cross section. At an e^+e^- collider with $\sqrt{s} = 1$ TeV, on the other hand, these backgrounds are at most of the size of the signal. Thus, requiring three or more b-tags may improve the sensitivity to λ at a 1 TeV e^+e^- collider. For $\sqrt{s} = 0.5$ TeV, the dramatically increased background may well lead to a decreased sensitivity, despite the gain in the signal cross section.

The results shown in Figs. 3 and 4 assume the efficiencies and misidentification probabilities of Eq. (8). A reduction of a factor 5 or more in most backgrounds can be achieved if one is willing to accept a slightly reduced b-tagging efficiency; see Eq. (9). A detailed analysis of the sensitivity limits which one may hope to achieve requiring four tagged b-quarks, or three or more tagged b's using the efficiencies of Eq. (8) or Eq. (9) will be presented in Sec. VI. The cross sections for the two sets of efficiencies and misidentification probabilities, and the SM signal, $e^+e^- \to jjb\bar{b}b\bar{b}$ including the full set of $\mathcal{O}(\alpha^6)$, $\mathcal{O}(\alpha_s^4\alpha^2)$ and $\mathcal{O}(\alpha_s^2\alpha^4)$ Feynman diagrams, and the backgrounds are listed in Table I for three and four tagged b-jets, together with the cross section for ≥ 3 b-tags.

One may wonder to what extent the renormalization scale uncertainty affects the cross sections listed in Table I. The reducible backgrounds are all of $\mathcal{O}(\alpha_s^4\alpha^2)$ and thus are uncertain by a factor $2^{\pm 1}$ or so. In the $e^+e^- \to jjb\bar{b}b\bar{b}$ cross section which has been calculated using the full set of $\mathcal{O}(\alpha^6)$, $\mathcal{O}(\alpha_s^4\alpha^2)$ and $\mathcal{O}(\alpha_s^2\alpha^4)$ Feynman diagrams, the $\mathcal{O}(\alpha_s^4\alpha^2)$ diagrams play an important role only for $\sqrt{s} = 0.5$ TeV and $m_H = 140$ GeV. In this case, I estimate that the scale uncertainty may change the cross section by a factor $1.5^{\pm 1}$.

Table I shows that, for $m_H = 120$ GeV, $jjb\bar{b}b\bar{b}$ production with four tagged b-quarks provides a clean, albeit low statistics, signal with a relatively small background. Including

the final state with three b-tags increases the signal cross section by almost 50%. While the background is still small for $\sqrt{s} = 1$ TeV, it becomes substantial for $\sqrt{s} = 0.5$ TeV. The signal to background ratio for $\sqrt{s} = 0.5$ TeV may be improved by choosing an optimal combination of b-tagging efficiency and light quark/gluon jet and charm quark misidentification probability [28]. Furthermore, in absence of a calculation of the NLO QCD corrections for $jjb\bar{b}c\bar{c}$, $b\bar{b}cjjj$ and $b\bar{b}4j$ production, the background cross section is subject to a large renormalization scale uncertainty. For $m_H = 140$ GeV, the signal cross section is so small that even with an integrated luminosity of several ab^{-1}, only a handful of signal events is produced.

For $\sqrt{s} = 1$ TeV, the background is already small for the efficiencies listed in Eq. (8) and not much is gained by choosing a different combination of b-tagging efficiency and light quark/gluon jet and charm quark misidentification probability.

The signal cross section may be further increased by relaxing the number of b-tagged jets to two. In this case, one of the Higgs bosons may undergo the decay $H \to c\bar{c}$ or $H \to gg$. For $m_H = 120$ GeV, this increases the signal cross section by about a factor 1.3. Unfortunately, the backgrounds increase by a much larger factor, and overwhelm the signal [54]. I therefore do not analyze the $ZHH \to b\bar{b}4j$ signal here.

For $m_H \geq 140$ GeV, the relatively small branching ratio of $B(H \to b\bar{b}) \approx 30\%$ makes it difficult to measure λ in $jjb\bar{b}b\bar{b}$ production, regardless of the b-tagging efficiency. In this Higgs mass range, $B(H \to W^*W) \approx 50\%$ and final states such as $b\bar{b}6j$ and $\ell^\pm\nu b\bar{b}4j$ offer the possibility to more than double the number of observed ZHH events. I do not investigate these final states here. For $m_H > 2M_W$, most Higgs bosons decay into a pair of W bosons. While there is not enough phase space for ZHH production in this region at a 500 GeV e^+e^- collider, a small number of ZHH events may be produced for $\sqrt{s} = 1$ TeV or above. However, as I will show in the following Section, the cross section for $\nu\bar{\nu}HH$ production is considerably larger in this region. ZHH production, therefore, is not discussed here for $m_H > 2M_W$.

V. $\nu\bar{\nu}HH$ ANALYSIS

For $\sqrt{s} \geq 1$ TeV, $e^+e^- \to \nu\bar{\nu}HH$ ($\nu = \nu_e$, ν_μ, ν_τ) becomes the dominant source of Higgs boson pairs. For $\nu = \nu_\mu$, ν_τ only ZHH production with $Z \to \bar{\nu}_\mu\nu_\mu$, $\bar{\nu}_\tau\nu_\tau$ contributes. For $\nu = \nu_e$, a total of eight Feynman diagrams contribute, including four ZHH, $Z \to \bar{\nu}_e\nu_e$ and four vector boson fusion diagrams. In the following, I will discuss $\nu\bar{\nu}HH$ production and the relevant backgrounds for $m_H = 120$ GeV, 140 GeV and $m_H = 180$ GeV, and $\sqrt{s} = 1$ TeV and 3 TeV.

A. $m_H = 120$ GeV

For $m_H = 120$ GeV, $H \to b\bar{b}$ decays dominate. I will therefore concentrate on the $\nu\bar{\nu}b\bar{b}b\bar{b}$ final state. Specifically, I require events with missing transverse momentum and four jets satisfying Eq. (6). A minimum of three of the jets have to be tagged as b-jets, and there have to be at least two jet pairs fulfilling Eq. (11).

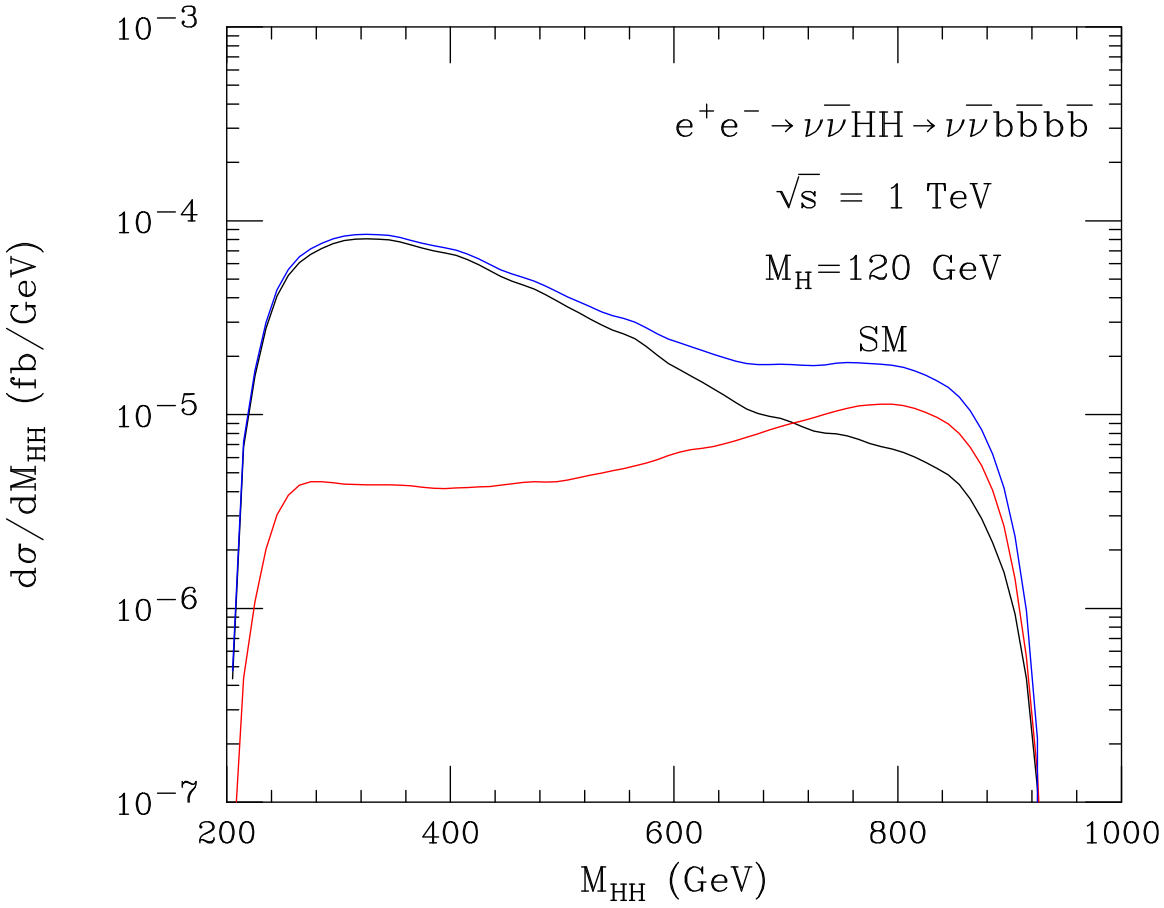

FIG. 5. The SM $e^+e^- \to \nu\bar{\nu}HH \to \nu\bar{\nu}4b$ cross section with three b-tags as a function of the Higgs pair invariant mass, M_{HH}, for $\sqrt{s} = 1$ TeV. The black (red) solid line shows the $ZHH \to \nu_l\bar{\nu}_l b\bar{b}b\bar{b}$ ($l = \mu, \tau$) ($e^+e^- \to \nu_e\bar{\nu}_e HH \to \nu_e\bar{\nu}_e b\bar{b}b\bar{b}$) cross section. The blue curve represents the total $e^+e^- \to \nu\bar{\nu}HH \to \nu\bar{\nu}b\bar{b}b\bar{b}$ cross section. The cuts imposed and the efficiencies used are summarized in Eqs. (6), (8), (10), and (11).

The SM $ZHH \to \nu_l\bar{\nu}_l b\bar{b}b\bar{b}$ ($l = \mu, \tau$) and $e^+e^- \to \nu_e\bar{\nu}_e HH \to \nu_e\bar{\nu}_e b\bar{b}b\bar{b}$ M_{HH} differential cross sections for $\sqrt{s} = 1$ TeV are shown by the solid black and red lines in Fig. 5. The blue line gives the inclusive $e^+e^- \to \nu\bar{\nu}HH \to \nu\bar{\nu}b\bar{b}b\bar{b}$ cross section. For small values of M_{HH}, the cross section is completely dominated by the process $e^+e^- \to \nu_e\bar{\nu}_e HH$, whereas for large Higgs pair invariant masses, ZHH production followed by $Z \to \nu_l\bar{\nu}_l$ gives the largest contribution to the inclusive $\nu\bar{\nu}HH$ cross section. A qualitatively similar result is obtained at $\sqrt{s} = 3$ TeV, however, with the $e^+e^- \to \nu_e\bar{\nu}_e HH$ cross section being more than a factor 100 larger than the ZHH rate at small values of M_{HH}.

The main backgrounds to $\nu\bar{\nu}HH \to \nu\bar{\nu}b\bar{b}b\bar{b}$ production are $e^+e^- \to \nu\bar{\nu}b\bar{b}b\bar{b}$ at $\mathcal{O}(\alpha_s^2\alpha^4)$ and $\mathcal{O}(\alpha^6)$ (about 2,300 single- and non-resonant Feynman diagrams), and $\nu\bar{\nu}b\bar{b}c\bar{c}$ (about 900 $\mathcal{O}(\alpha_s^2\alpha^4)$ and $\mathcal{O}(\alpha^6)$ Feynman diagrams) and $\nu\bar{\nu}b\bar{b}jj$ production (about 2,100 $\mathcal{O}(\alpha_s^2\alpha^4)$ and $\mathcal{O}(\alpha^6)$ Feynman diagrams) where one or two charm or light quark/gluon jets are mistagged. Potentially dangerous backgrounds also come from $b\bar{b}b\bar{b}$ and $b\bar{b}jj$ production with the missing transverse originating from the energy loss in b-decays or jet energy mismeasurements.

The Higgs-pair invariant mass distribution for $\sqrt{s} = 1$ TeV and 3 TeV for the SM $\nu\bar{\nu}HH$ signal (solid black curve), $\Delta\lambda_{HHH} = +1$ (dashed black line), $\Delta\lambda_{HHH} = -1$ (dotted black line), the full set of $\mathcal{O}(\alpha_s^2\alpha^4)$ and $\mathcal{O}(\alpha^6)$ $\nu\bar{\nu}b\bar{b}b\bar{b}$ diagrams (magenta line), and the relevant background processes is shown in Fig. 6. In ZHH production, positive (moderately negative) values of $\Delta\lambda_{HHH}$ increase (decrease) the cross section. The opposite is true for $\nu\bar{\nu}HH$ production. For $\Delta\lambda_{HHH} = -1$, the cross section is strongly enhanced, while for $\Delta\lambda_{HHH} = +1$ it is somewhat smaller than the SM cross section over much of the M_{HH} range. Only near the HH threshold is the cross section larger than in the SM. As in the ZHH case, the deviations from the SM are largely concentrated at small values of M_{HH}. Comparison with Fig. 2 shows that the cross section for $\nu\bar{\nu}b\bar{b}b\bar{b}$ production is a few times larger than that for $jjb\bar{b}b\bar{b}$ production at $\sqrt{s} = 1$ TeV.

When the full set of $\mathcal{O}(\alpha_s^2\alpha^4)$ and $\mathcal{O}(\alpha^6)$ diagrams instead of the $\nu\bar{\nu}HH$ signal diagrams is used to calculate the $\nu\bar{\nu}b\bar{b}b\bar{b}$ cross section, the resulting differential cross section is reduced by $10-20\%$, except for the HH threshold region, where it is enhanced. It is thus relatively easy to confuse the effects of single- and non-resonant Feynman diagrams and those of moderately positive anomalous Higgs self-couplings.

The $\nu\bar{\nu}b\bar{b}c\bar{c}$ and $\nu\bar{\nu}b\bar{b}jj$ backgrounds are found to be at least one order of magnitude smaller than the signal for the efficiencies used here. Due to the renormalization scale uncertainty, the cross sections for these processes may vary by $\mathcal{O}(30-40\%)$. The $b\bar{b}b\bar{b}$ and $b\bar{b}jj$ backgrounds are largest for M_{HH} close to the kinematic boundary, $\sqrt{s}$, and drop rapidly for smaller values of M_{HH}. This is easily understood. In both cases, the invariant mass of the $b\bar{b}b\bar{b}$ system equals the center of mass energy if the energy loss due to b-quark decays and jet mismeasurements are not taken into account. While these backgrounds are substantial for $M_{HH} > 850$ GeV at a 1 TeV machine, they decrease rapidly with increasing values of $\sqrt{s}$.

The $b\bar{b}b\bar{b}$ and $b\bar{b}jj$ backgrounds are concentrated at large values of M_{HH}, whereas anomalous Higgs boson self-couplings mostly affect the cross section for small values of the Higgs pair invariant mass. These backgrounds thus have little or no effect on the sensitivity limits for λ_{HHH}. Since the region of large Higgs pair invariant masses is largely insensitive to λ_{HHH}, measuring the cross section in this region would make it possible to normalize the cross section. Unfortunately, the $e^+e^- \to \nu\bar{\nu}HH \to \nu\bar{\nu}b\bar{b}b\bar{b}$ cross section falls very quickly with increasing Higgs pair invariant mass, in particular for higher center of mass energies, resulting in a large statistical uncertainty in the large M_{HH} region. Accurate theoretical predictions of the SM $\nu\bar{\nu}b\bar{b}b\bar{b}$ cross section thus will be indispensable for a measurement of the Higgs boson self-coupling in this final state.

B. $m_H = 140$ GeV

The branching ratio for $H \to b\bar{b}$ drops rather quickly with increasing Higgs boson mass and, for $m_H = 140$ GeV, only about 1/3 of the Higgs bosons decay into $b\bar{b}$. At the same time, the $H \to W^*W \to 4f$ branching ratio increases to about 50%. The $4f$ final state consists of four jets with a probability of about 46% while the $\ell\nu_\ell jj$ ($\ell = e, \mu$) final state has a branching ratio of about 29%. All other final states have a combined branching ratio of 25%. This suggests to consider the $\nu\bar{\nu}b\bar{b}4j$, $\nu\bar{\nu}b\bar{b}\ell\nu_\ell jj$, $\nu\bar{\nu}8j$ and $\nu\bar{\nu}\ell\nu_\ell 6j$ final states in addition to $\nu\bar{\nu}b\bar{b}b\bar{b}$ production. Since the decay $HH \to b\bar{b}4j$ has the largest individual branching

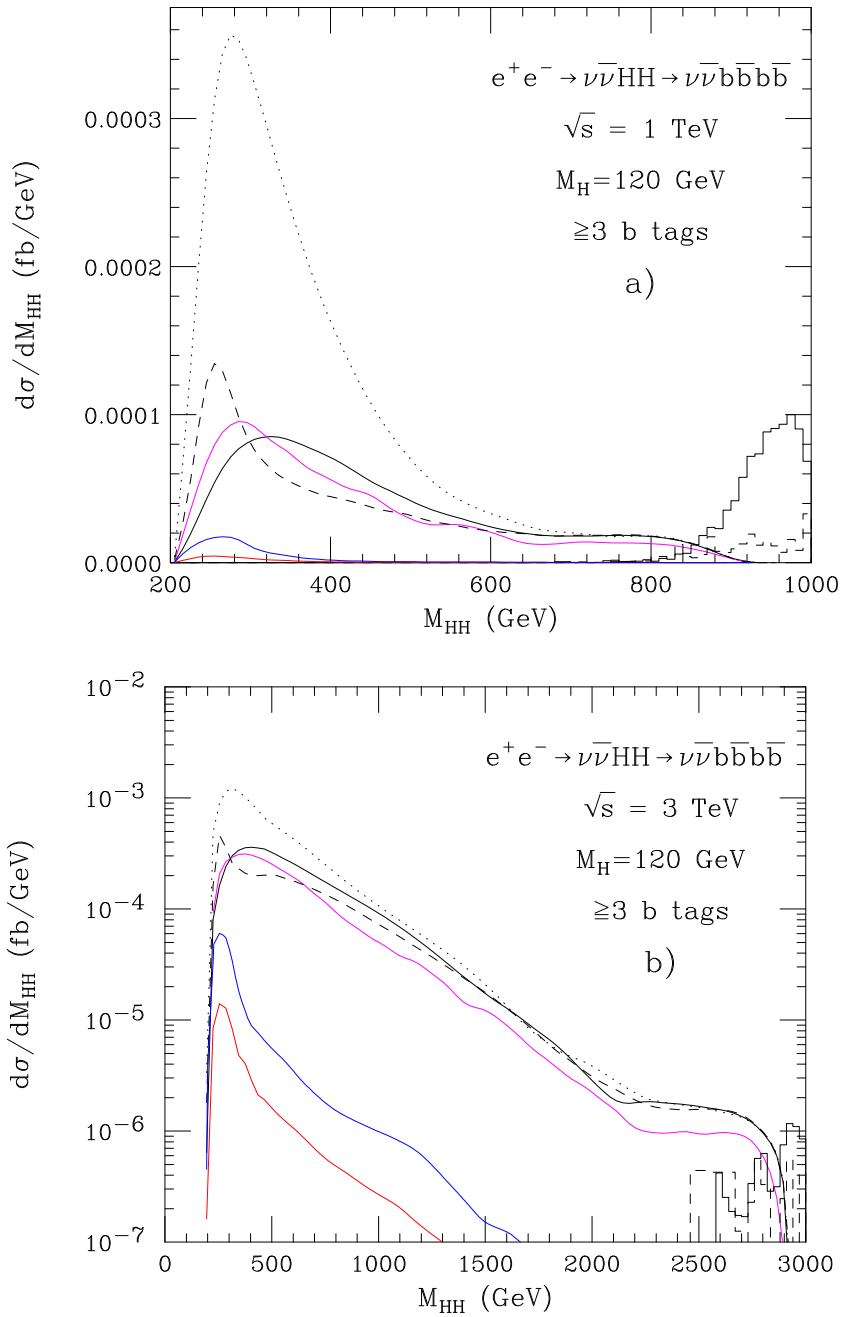

FIG. 6. The $e^+e^- \to \nu\bar{\nu}HH \to \nu\bar{\nu}b\bar{b}b\bar{b}$ cross section with three or more b-tags as a function of the Higgs pair invariant mass, M_{HH}, for $m_H = 120$ GeV and a) $\sqrt{s} = 1$ TeV and b) $\sqrt{s} = 3$ TeV. The black solid line is the prediction of the SM signal cross section. The black dashed and dotted lines correspond to the $\nu\bar{\nu}HH$ signal cross section for $\Delta\lambda_{HHH} = +1$ and $\Delta\lambda_{HHH} = -1$, respectively. The magenta line shows the SM cross section for $e^+e^- \to \nu\bar{\nu}b\bar{b}b\bar{b}$ including the full set of $\mathcal{O}(\alpha^6)$ and $\mathcal{O}(\alpha_s^2\alpha^4)$ Feynman diagrams. The blue and red lines correspond to the $\nu\bar{\nu}b\bar{b}c\bar{c}$ and $\nu\bar{\nu}b\bar{b}jj$ cross section. The solid and dashed histograms represent the prediction of the $b\bar{b}b\bar{b}$ and $b\bar{b}jj$ backgrounds. The cuts imposed and the efficiencies used are summarized in Eqs. (6), (8), (10), and (11).

fraction of all Higgs pair decays for $m_H = 140$ GeV, I will consider $\nu\bar{\nu}b\bar{b}4j$ production in addition to the $\nu\bar{\nu}b\bar{b}b\bar{b}$ final state in this Section.

The results for $\nu\bar{\nu}b\bar{b}b\bar{b}$ production with $m_H = 140$ GeV are shown in Fig. 7. I impose the same cuts as in Sec. V A, except for the cut on $m(b\bar{b})$ which is replaced by that of Eq. (12). Taking the full set of $\mathcal{O}(\alpha^6)$ and $\mathcal{O}(\alpha_s^2\alpha^4)$ Feynman diagrams into account in the calculation considerably enhances the cross section (magenta line) in the HH threshold region, while it reduces the $\nu\bar{\nu}b\bar{b}b\bar{b}$ rate by about 20% for larger values of M_{HH}. The effect of the non-signal diagrams contributing to $\nu\bar{\nu}b\bar{b}b\bar{b}$ production can be easily confused with that of a positive anomalous Higgs self-coupling. The $\nu\bar{\nu}b\bar{b}c\bar{c}$ background is substantial in the HH threshold region, but falls very quickly with the Higgs pair invariant mass, and becomes negligible for $M_{HH} > 400$ GeV. The $\nu\bar{\nu}b\bar{b}jj$ background is about a factor four smaller than that originating from $\nu\bar{\nu}b\bar{b}c\bar{c}$ production for the efficiencies used here. $b\bar{b}jj$ and $b\bar{b}b\bar{b}$ production constitute an important background for $M_{HH} > 800$ GeV ($M_{HH} > 2.5$ TeV) at $\sqrt{s} = 1$ TeV ($\sqrt{s} = 3$ TeV).

When calculating the cross section for $\nu\bar{\nu}HH \to \nu\bar{\nu}b\bar{b}4j$ production care has to be taken. In addition to $H \to W^*W \to 4j$, $H \to Z^*Z \to 4j$ also contributes, albeit with a much smaller branching ratio ($B(H \to Z^*Z) \approx 10\%$ vs. $B(H \to W^*W) \approx 50\%$ for $m_H = 140$ GeV). To select $\nu\bar{\nu}HH \to \nu\bar{\nu}b\bar{b}4j$ events, I require, in addition to the standard jet and missing transverse momentum cuts of Eqs. (6), two tagged b-quarks satisfying Eq. (11) and four non-tagged jets with an invariant mass

$$|m_H - m(4j)| < 20 \text{ GeV}. \tag{15}$$

One un-tagged jet pair has to be consistent with originating from a W decay (see Eq. (10)).

The main reducible backgrounds originate from $\nu\bar{\nu}6j$ production where two jets are mistagged as b-quarks, $\nu\bar{\nu}c\bar{c}4j$ production where both charm quarks are misidentified as b's, and from $e^+e^- \to b\bar{b}4j$ with the missing transverse momentum originating from jet mismeasurements and the energy loss arising from b-decays. Furthermore, non-resonant $\nu\bar{\nu}b\bar{b}4j$ production constitutes a potentially dangerous irreducible background.

With the exception of $e^+e^- \to b\bar{b}4j$, these are processes with eight particles in the final state. I have attempted to calculate the $e^+e^- \to \nu\bar{\nu}b\bar{b}4j$ cross section including the full set of $\mathcal{O}(\alpha_s^4\alpha^4)$, $\mathcal{O}(\alpha_s^2\alpha^6)$ and $\mathcal{O}(\alpha^8)$ diagrams using several publically available programs. Generating the contributing Feynman diagrams via `MadGraph` [44] resulted in well over 10^5 Feynman diagrams and took more than 200 hours of CPU time on a 3ghz Xeon workstation. The evaluation of the cross section for this process using `MadEvent` would require computing resources significantly larger than those available, and therefore was not attempted. Like `MadEvent`, the current version of `Sherpa` [55] is based on a Feynman diagrammatic approach [56], and thus is expected to be too slow to calculate the cross section of $2 \to 8$ processes. In the future, `Sherpa` will use [57] `COMIX` [58], a new matrix element generator which is based on color dressed Berends-Giele recursive relations [59]. This should allow for a much faster evaluation of matrix elements, and thus make it possible to calculate the cross sections of processes with ≥ 8 particles in the final state.

For processes with many particles in the final state, `WHIZARD` [60] and `HELAC-PHEGAS` [61] are potential alternatives to `MadEvent` and `Sherpa`. `WHIZARD` uses `O'Mega` [62] which implements an algorithm that collects all common sub-expressions in the sum over Feynman diagrams contributing to a given scattering amplitude at tree level. `HELAC-PHEGAS` calculates

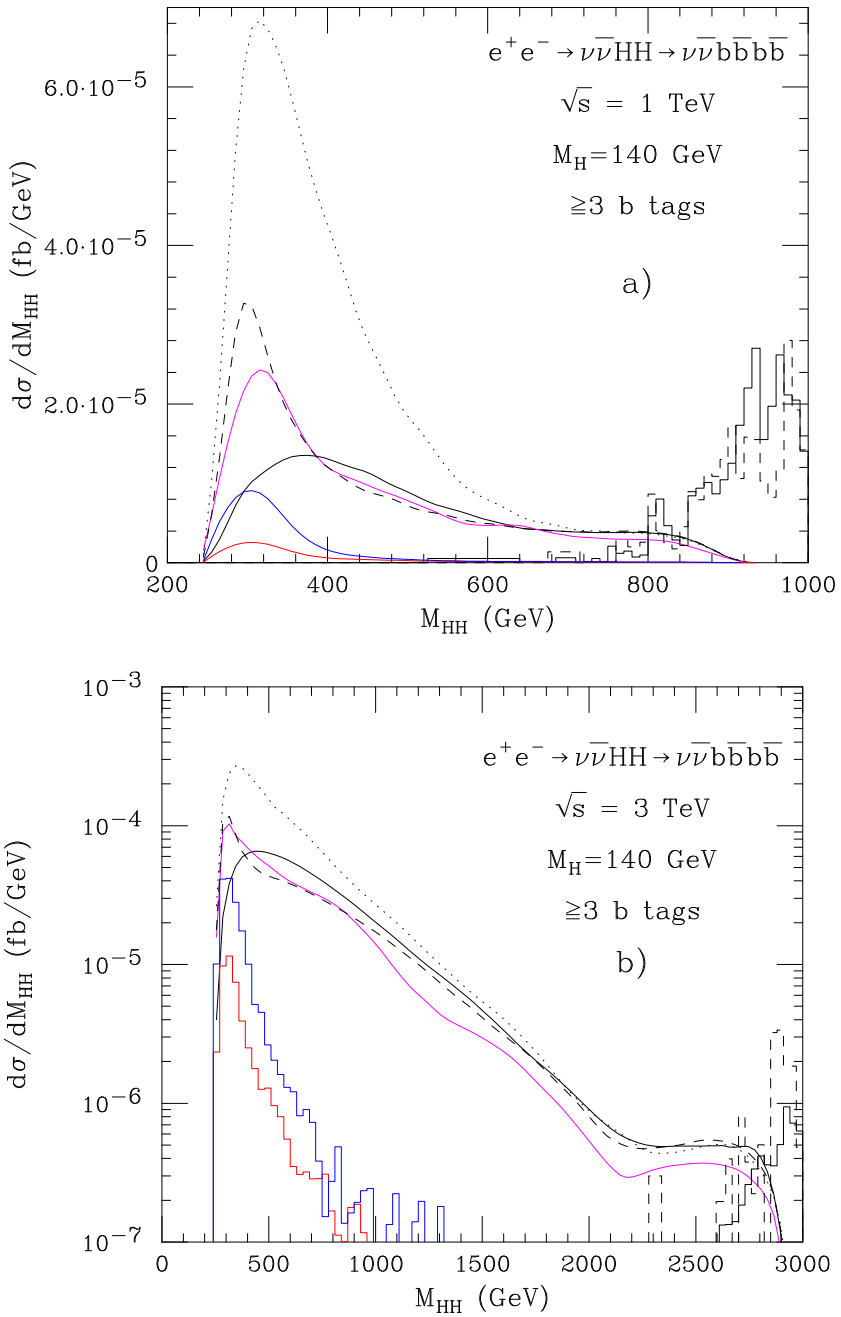

FIG. 7. The $e^+e^- \to \nu\bar{\nu}HH \to \nu\bar{\nu}b\bar{b}b\bar{b}$ cross section with three or more b-tags as a function of the Higgs pair invariant mass, M_{HH}, for $m_H = 140$ GeV and a) $\sqrt{s} = 1$ TeV and b) $\sqrt{s} = 3$ TeV. The black solid line is the prediction of the SM signal cross section. The black dashed and dotted lines correspond to the $\nu\bar{\nu}HH$ signal cross section for $\Delta\lambda_{HHH} = +1$ and $\Delta\lambda_{HHH} = -1$, respectively. The magenta line shows the SM cross section for $e^+e^- \to \nu\bar{\nu}b\bar{b}b\bar{b}$ including the full set of $\mathcal{O}(\alpha^6)$ and $\mathcal{O}(\alpha_s^2\alpha^4)$ Feynman diagrams. The blue and red lines/histograms correspond to the $\nu\bar{\nu}b\bar{b}c\bar{c}$ and $\nu\bar{\nu}b\bar{b}jj$ cross section. The solid and dashed histograms represent the prediction of the $b\bar{b}b\bar{b}$ and $b\bar{b}jj$ backgrounds. The cuts imposed and the efficiencies used are summarized in Eqs. (6), (8), (10), and (12).

matrix elements using recursive Schwinger-Dyson equations. I have attempted to compute the $e^+e^- \to \nu\bar{\nu}b\bar{b}4j$ cross section using `WHIZARD` and `HELAC-PHEGAS`. The compilation of the `WHIZARD` code was terminated without a result after more than 40 hours of CPU time on a 3ghz Xeon workstation. The `HELAC-PHEGAS` code compiled successfully, but failed to run with an error in an underlying basic linux library. Another program which may be able to handle a process such as $e^+e^- \to \nu\bar{\nu}b\bar{b}4j$ is `carlomat` [63], which, however, is not publically available yet.

One can argue that a substantial portion of the contribution of the non-resonant $\mathcal{O}(\alpha_s^2\alpha^6)$ and $\mathcal{O}(\alpha^8)$ diagrams[1] to the $\nu\bar{\nu}b\bar{b}4j$ cross section originates from the off-shell $W^* \to jj$ jet pair. This suggests that calculating the $e^+e^- \to \nu\bar{\nu}Wjjb\bar{b}$ cross section with $W \to jj$, or the $\nu\bar{\nu}H4j$ cross section with $H \to b\bar{b}$, may be sufficient for an estimate of how non-resonant diagrams affect the $\nu\bar{\nu}b\bar{b}4j$ rate. Results based on a calculation of the process $e^+e^- \to \nu\bar{\nu}Wjjb\bar{b}$ with $W \to jj$ (about 7,000 $\mathcal{O}(\alpha_s^2\alpha^5)$ and $\mathcal{O}(\alpha^7)$ diagrams) are shown in Fig. 8. The black solid line is the prediction of the SM signal cross section; the black dashed and dotted lines correspond to the $\nu\bar{\nu}HH$ signal cross section for $\Delta\lambda_{HHH} = +1$ and $\Delta\lambda_{HHH} = -1$, respectively. With the acceptance cuts imposed here, the $\nu\bar{\nu}b\bar{b}4j$ cross section is approximately as large as that for $\nu\bar{\nu}b\bar{b}b\bar{b}$ production. The $e^+e^- \to \nu\bar{\nu}Wjjb\bar{b}$, $W \to jj$, cross section is shown by the red line. While the non-resonant QCD and electroweak diagrams included in $e^+e^- \to \nu\bar{\nu}Wjjb\bar{b}$, $W \to jj$, have a fairly small effect at small values of M_{HH}, they are seen to reduce the differential cross section by about 30% in the large Higgs pair invariant mass region. The non-resonant diagrams not included in $\nu\bar{\nu}Wjjb\bar{b}$, $W \to jj$ may well affect the cross section to a similar degree.

I have not attempted to compute the $\nu\bar{\nu}c\bar{c}4j$ and $\nu\bar{\nu}6j$ backgrounds, suspecting that one would run into problems similar to those encountered for $e^+e^- \to \nu\bar{\nu}b\bar{b}4j$. I expect that these backgrounds are small compared with the signal, as in the case of the analogous $\nu\bar{\nu}b\bar{b}c\bar{c}$ and $\nu\bar{\nu}4j$ backgrounds in $\nu\bar{\nu}b\bar{b}b\bar{b}$ production.

The $e^+e^- \to b\bar{b}4j$ background (with about 15,000 $\mathcal{O}(\alpha^6)$, $\mathcal{O}(\alpha_s^2\alpha^4)$ and $\mathcal{O}(\alpha_s^4\alpha^2)$ Feynman diagrams contributing) with the missing transverse momentum originating from jet mismeasurements and the energy loss arising from b-decays was found to be very small for the cuts imposed.

C. $m_H = 180$ GeV

For $m_H = 180$ GeV, almost all Higgs bosons decay into a pair of W-bosons ($B(H \to W^+W^-) \approx 93\%$). Subsequent W decay then leads to $HH \to \ell^\pm\nu_\ell 6j$ ($\ell = e, \mu$) with a branching ratio of about 24%, or $HH \to 8j$ with a branching fraction of $\approx 19\%$. Since the individual branching ratios for all other final states are significantly smaller, I shall concentrate on $HH \to \ell^\pm\nu_\ell 6j$ and $HH \to 8j$ here.

If one of the four W-bosons decays leptonically, the final state consists of one charged lepton, six jets and missing transverse momentum which originates from the three neutrinos in the event. The main backgrounds originate from single resonant and non-resonant $e^+e^- \to$

[1] There are no $\mathcal{O}(\alpha_s^4\alpha^4)$ diagrams contributing to the process.

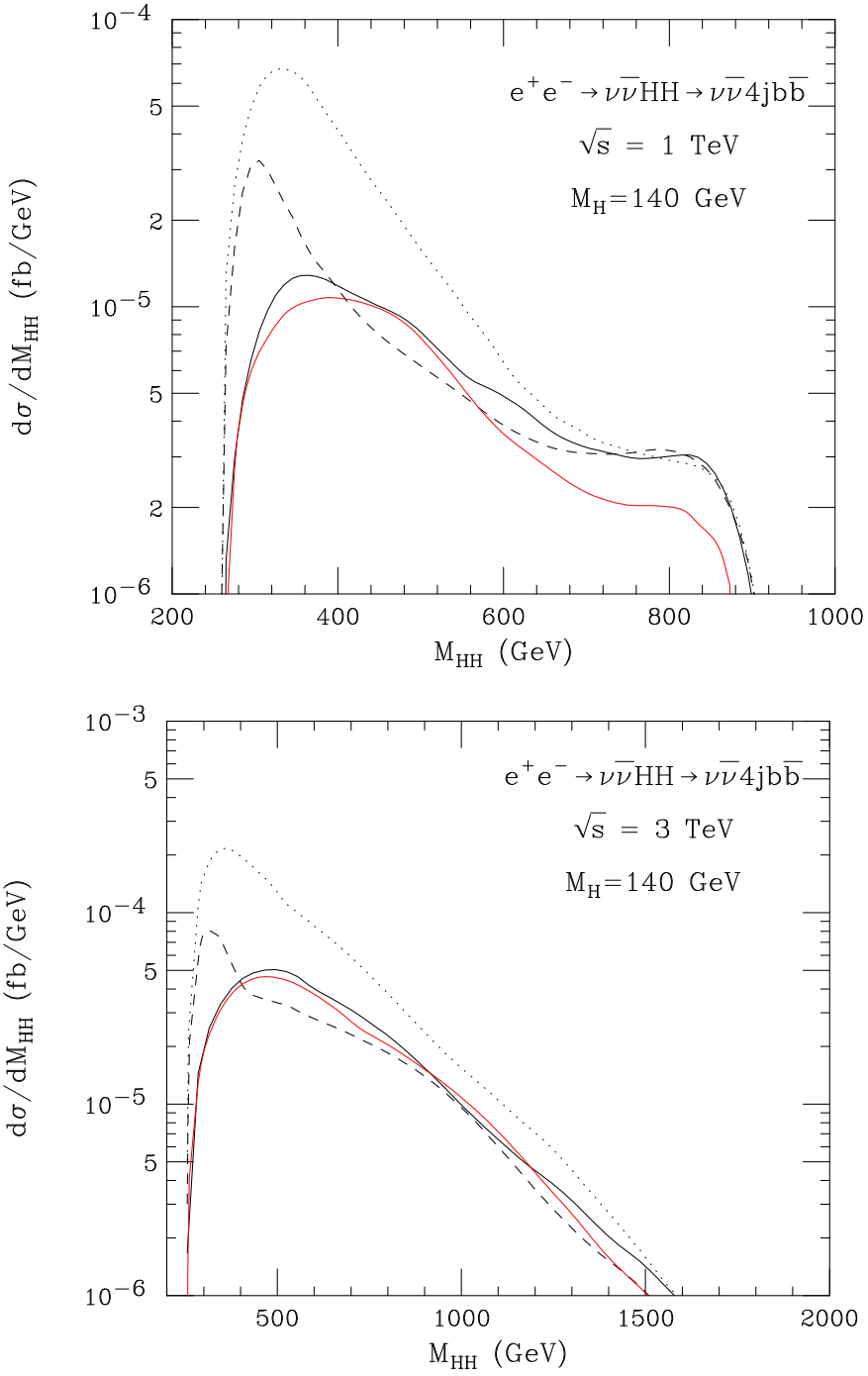

FIG. 8. The $e^+e^- \to \nu\bar{\nu}HH \to \nu\bar{\nu}b\bar{b}4j$ cross section as a function of the Higgs pair invariant mass, M_{HH}, for $m_H = 140$ GeV and a) $\sqrt{s} = 1$ TeV and b) $\sqrt{s} = 3$ TeV. The black solid line is the prediction of the SM signal cross section. The black dashed and dotted lines correspond to the $\nu\bar{\nu}HH$ signal cross section for $\Delta\lambda_{HHH} = +1$ and $\Delta\lambda_{HHH} = -1$, respectively. The red line shows the SM cross section for $e^+e^- \to \nu\bar{\nu}Wjjb\bar{b}$, $W \to jj$, including the full set of $\mathcal{O}(\alpha^7)$ and $\mathcal{O}(\alpha_s^2\alpha^5)$ Feynman diagrams. The cuts imposed and the efficiencies used are summarized in Eqs. (6), (8), (10), (11), and (15).

$\nu\bar{\nu}\ell^{\pm}\nu_\ell 6j$ diagrams and $W^{\pm}6j$ production (with approximately 21,000 $\mathcal{O}(\alpha^3\alpha_s^4)$ Feynman diagrams contributing). In order to identify $\nu\bar{\nu}HH$ events in the $\ell^{\pm}\not{p}_T 6j$ final state, I require, in addition to the standard lepton, jet and $\not{p}_T$ identification cuts of Eq. (6), three or more jet pairs which satisfy Eq. (10) with two of the jet pairs having an invariant mass in the range

$$160 \text{ GeV} < m([jj][jj]) < 200 \text{ GeV}. \tag{16}$$

Since the invariant mass of the Higgs pair cannot easily be reconstructed, I consider the distribution of the invariant mass of the six jets, M_{6j}, instead.

Although a full calculation of the $2 \to 10$ process $e^+e^- \to \nu\bar{\nu}\ell^{\pm}\nu_\ell 6j$ is currently not feasible, it is still possible to get an idea of how strongly non-resonant diagrams affect the $6j$ invariant mass distribution by calculating the cross sections of the processes $e^+e^- \to \nu\bar{\nu}\ell\nu_\ell jjH$ with $H \to W^+W^- \to 4j$ (with approximately 1,300 $\mathcal{O}(\alpha^7)$ Feynman diagrams contributing), and $e^+e^- \to \nu\bar{\nu}4jH$ with $H \to W^+W^- \to \ell\nu_\ell jj$ (with approximately 20,000 $\mathcal{O}(\alpha^7)$ and $\mathcal{O}(\alpha^5\alpha_s^2)$ Feynman diagrams contributing). In Fig. 9, I show the SM $e^+e^- \to \nu_e\bar{\nu}_e HH \to \nu_e\bar{\nu}_e\ell^{\pm}\nu_\ell 6j$ M_{6j} differential cross section for the signal at $\sqrt{s} = 1$ TeV, together with the results for $\nu_e\bar{\nu}_e\ell^{\pm}\nu_\ell jjH$, $H \to W^+W^- \to 4j$ production (red line), and $e^+e^- \to \nu_e\bar{\nu}_e 4jH$, $H \to W^+W^- \to \ell\nu_\ell jj$ (blue curve). Similar results are obtained for $\sqrt{s} = 3$ TeV, and for $e^+e^- \to \nu_l\bar{\nu}_l HH \to \nu_l\bar{\nu}_l\ell^{\pm}\nu_\ell 6j$ with $l = \mu$, τ.

The non-resonant diagrams in $e^+e^- \to \nu_e\bar{\nu}_e\ell^{\pm}\nu_\ell jjH$, $H \to W^+W^- \to 4j$ are found to significantly enhance the $\nu_e\bar{\nu}_e HH$ cross section near threshold. This is to be expected since the $\ell\nu_\ell$ invariant mass cannot be constrained; the presence of three neutrinos in the final state makes it impossible to use the $\ell\not{p}_T$ transverse mass to reduce the background from non-resonant diagrams. The non-resonant diagrams in $\nu_e\bar{\nu}_e 4jH$, $H \to W^+W^- \to \ell\nu_\ell jj$ production, on the other hand, reduce the cross section by a factor $1.5 - 2$ for the cuts imposed. An estimate of the effect of the full set of non-resonant diagrams may be obtained by averaging the $\nu_e\bar{\nu}_e\ell^{\pm}\nu_\ell jjH$, $H \to W^+W^- \to 4j$ and $\nu_e\bar{\nu}_e 4jH$, $H \to W^+W^- \to \ell\nu_\ell jj$ cross sections which is shown by the magenta line in Fig. 9.

The estimate obviously ignores a large number of non-resonant Feynman diagrams. As demonstrated by the blue line in Fig. 9, non-resonant Feynman diagrams may significantly affect the $\nu_e\bar{\nu}_e HH$ cross section, and one may worry whether the averaging procedure employed here does yield credible results. To justify the averaging procedure, I compare in Fig. 10 the SM $e^+e^- \to \nu_e\bar{\nu}_e\ell^{\pm}\nu_\ell jjH$, $H \to WW \to 4j$ M_{6j} distribution for $m_H = 180$ GeV and $\sqrt{s} = 3$ TeV (black dashed line) with the result obtained from averaging the $\nu_e\bar{\nu}_e\ell^{\pm}\nu_\ell WH$, $W \to jj$, $H \to WW \to 4j$ (blue line) and $\nu_e\bar{\nu}_e Wjj H$, $W \to \ell\nu_\ell$ $H \to WW \to 4j$ (black solid line) cross sections (red line). For comparison, the magenta line shows the $\nu_e\bar{\nu}_e HH$, $HH \to 4W \to \ell\nu_\ell 6j$ signal cross section. The red and black dashed lines agree within a few percent, lending credibility to the averaging procedure used in Fig. 9.

Adopting the averaging procedure introduced above, I show in Fig. 11 the $6j$ invariant mass distribution for the SM $e^+e^- \to \nu\bar{\nu}HH \to \nu\bar{\nu}\ell\nu_\ell 6j$ signal (solid black line), $\Delta\lambda_{HHH} = +1$ (dashed black line), and $\Delta\lambda_{HHH} = -1$ (dotted black line) for $\sqrt{s} = 1$ TeV and 3 TeV, together with the estimated $\nu\bar{\nu}\ell\nu_\ell 6j$ cross section including non-resonant diagrams (magenta lines). The non-resonant diagrams are seen to somewhat reduce the cross section over most of the $6j$ invariant mass range. Only for large values of M_{6j} do they increase the differential cross section. The blue hatched histogram in Fig. 11a shows the $W6j$ background. For

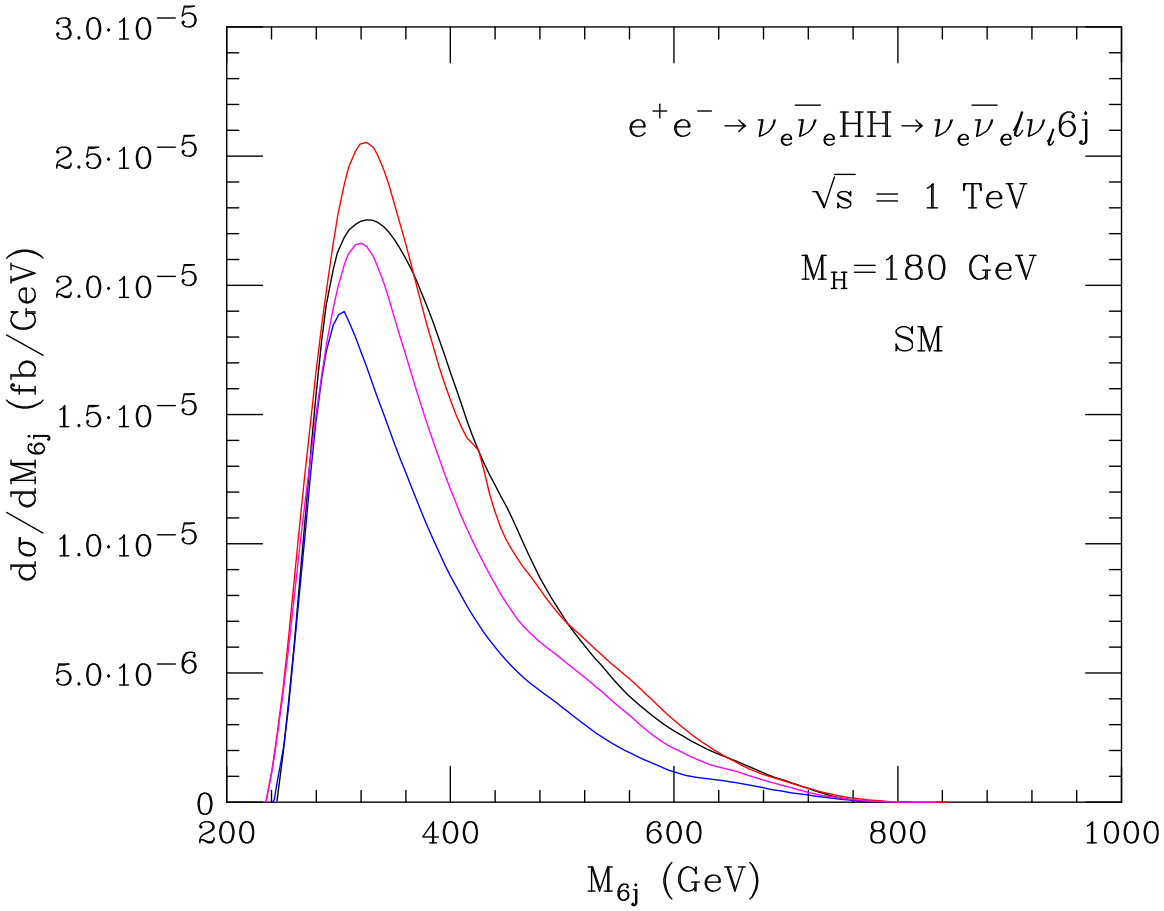

FIG. 9. The SM $e^+e^- \to \nu_e\bar{\nu}_e HH \to \nu_e\bar{\nu}_e\ell^\pm\nu_\ell 6j$ cross section as a function of the $6j$ invariant mass, M_{6j}, for $\sqrt{s} = 1$ TeV. The red line shows the $e^+e^- \to \nu_e\bar{\nu}_e\ell^\pm\nu_\ell jjH$, $H \to W^+W^- \to 4j$ cross section. The blue curve gives the $e^+e^- \to \nu_e\bar{\nu}_e 4jH$, $H \to W^+W^- \to \ell\nu_\ell jj$ cross section. The magenta line gives an estimate of the $e^+e^- \to \nu_e\bar{\nu}_e\ell^\pm\nu_\ell 6j$ cross section, obtained from averaging the $e^+e^- \to \nu_e\bar{\nu}_e\ell^\pm\nu_\ell jjH$, $H \to W^+W^- \to 4j$ and $e^+e^- \to \nu_e\bar{\nu}_e 4jH$, $H \to W^+W^- \to \ell\nu_\ell jj$ differential cross sections. The cuts imposed and the efficiencies used are summarized in Eqs. (6), (8), (10), and (16).

$\sqrt{s} = 3$ TeV the $W6j$ cross section is too small to show up for the range of cross sections displayed. Clearly, the $e^+e^- \to W6j$ background is negligible at both center of mass energies.

If all four W bosons in $HH \to 4W$ decay hadronically, the final state consists of eight jets and missing transverse momentum. To identify $\nu\bar{\nu}HH$ events in the $\not{p}_T 8j$ final state, I require, in addition to the standard $\not{p}_T$ and jet identification cuts of Eq. (6), four jet pairs which satisfy Eq. (10). Furthermore, the jet pairs are required to form two groups of four jet systems which satisfy Eq. (16). The four jets have to consist of two jet pairs with each jj system fulfilling Eq. (10).

The main background to the $\not{p}_T 8j$ final state originates from non-resonant diagrams which I estimate by calculating the cross section for $e^+e^- \to \nu\bar{\nu}4jH$ with $H \to WW \to 4j$ and employing the same averaging procedure as for the $\ell\not{p}_T 6j$ final state. The background from $e^+e^- \to 8j$ with the missing transverse momentum originating from jet mismeasurements

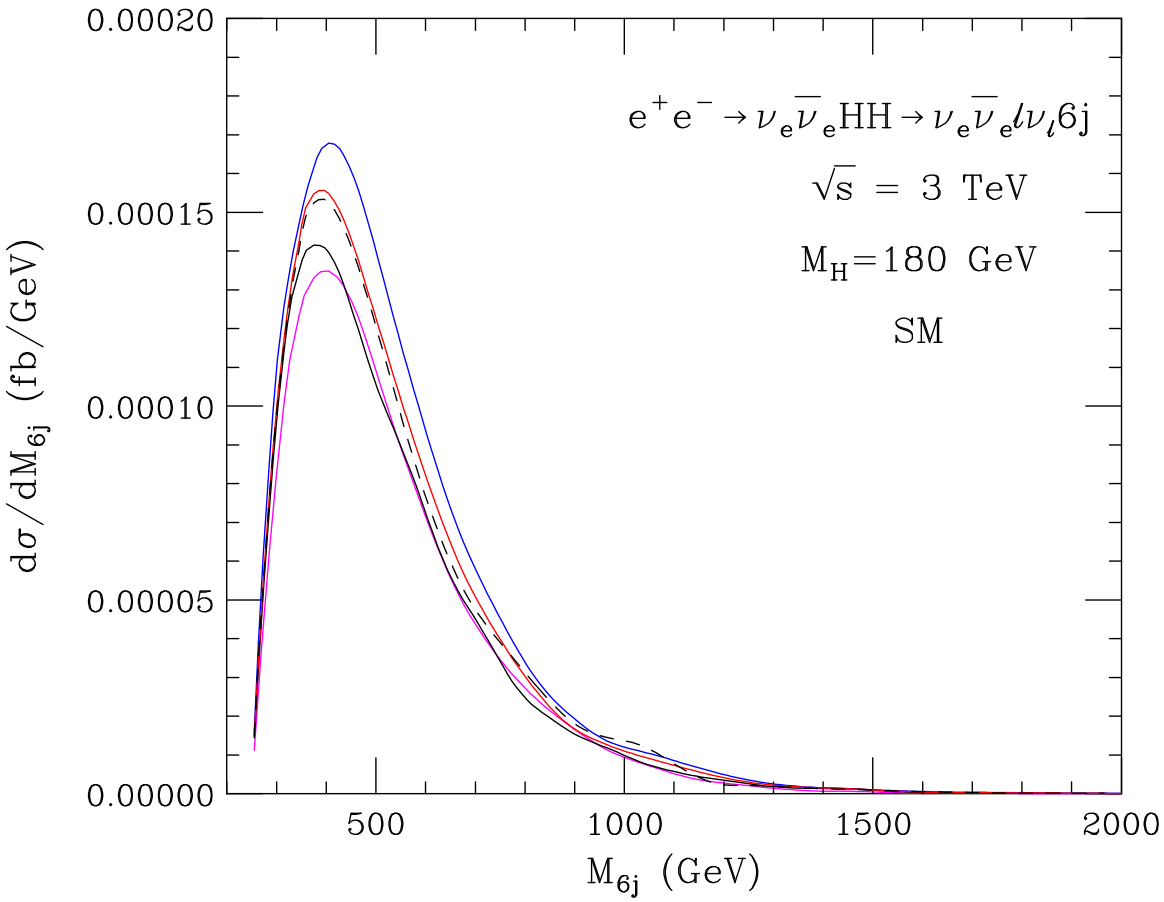

FIG. 10. The SM $e^+e^- \to \nu_e\bar{\nu}_e\ell^\pm\nu_\ell jjH$, $H \to WW \to 4j$ cross section as a function of the $6j$ invariant mass, M_{6j} for $\sqrt{s} = 3$ TeV (dashed black line). The black solid line shows the $\nu_e\bar{\nu}_e Wjj H$, $W \to \ell\nu_\ell$, $H \to WW \to 4j$ cross section. The blue curve gives the $\nu_e\bar{\nu}_e\ell^\pm\nu_\ell WH$, $W \to jj$, $H \to WW \to 4j$ cross section. The black dashed line gives an estimate of the $e^+e^- \to \nu_e\bar{\nu}_e\ell^\pm\nu_\ell jjH$, $H \to WW \to 4j$ cross section cross section from averaging the $\nu_e\bar{\nu}_e Wjj H$, $W \to \ell\nu_\ell$, $H \to WW \to 4j$ and $\nu_e\bar{\nu}_e\ell^\pm\nu_\ell WH$, $W \to jj$, $H \to WW \to 4j$ differential cross sections. For comparison, the magenta line shows the $\nu_e\bar{\nu}_e HH$, $HH \to 4W \to \ell\nu_\ell 6j$ signal cross section. The cuts imposed and the efficiencies used are summarized in Eqs. (6), (8), (10), and (16).

is expected to be small except for Higgs pair invariant masses close to $\sqrt{s}$. The results for the Higgs pair invariant mass distribution with $\sqrt{s} = 1$ TeV and 3 TeV are shown in Fig. 12. The non-resonant diagrams included in $e^+e^- \to \nu\bar{\nu}4jH$, $H \to WW \to 4j$, are seen to substantially reduce the cross section away from the threshold (magenta line). There is no guarantee that the averaging procedure used approximates the $\nu\bar{\nu}8j$ cross section including the full set of non-resonant Feynman diagrams with a similar accuracy as that observed for the $\nu\bar{\nu}\ell\nu_\ell 6j$ final state. The non-resonant diagrams ignored in $e^+e^- \to \nu\bar{\nu}4jH$, $H \to WW \to 4j$ may increase, or further decrease, the cross section. The main conclusion drawn from Fig. 12, therefore, is that non-resonant Feynman diagrams may substantially affect the $\nu\bar{\nu}8j$ cross section, and alter the shape of the M_{HH} distribution. The effect of non-resonant Feynman diagrams can of course be reduced by imposing a more stringent cut on the $4j$ invariant mass than that used here (see Eq. (16)). Whether this will be possible

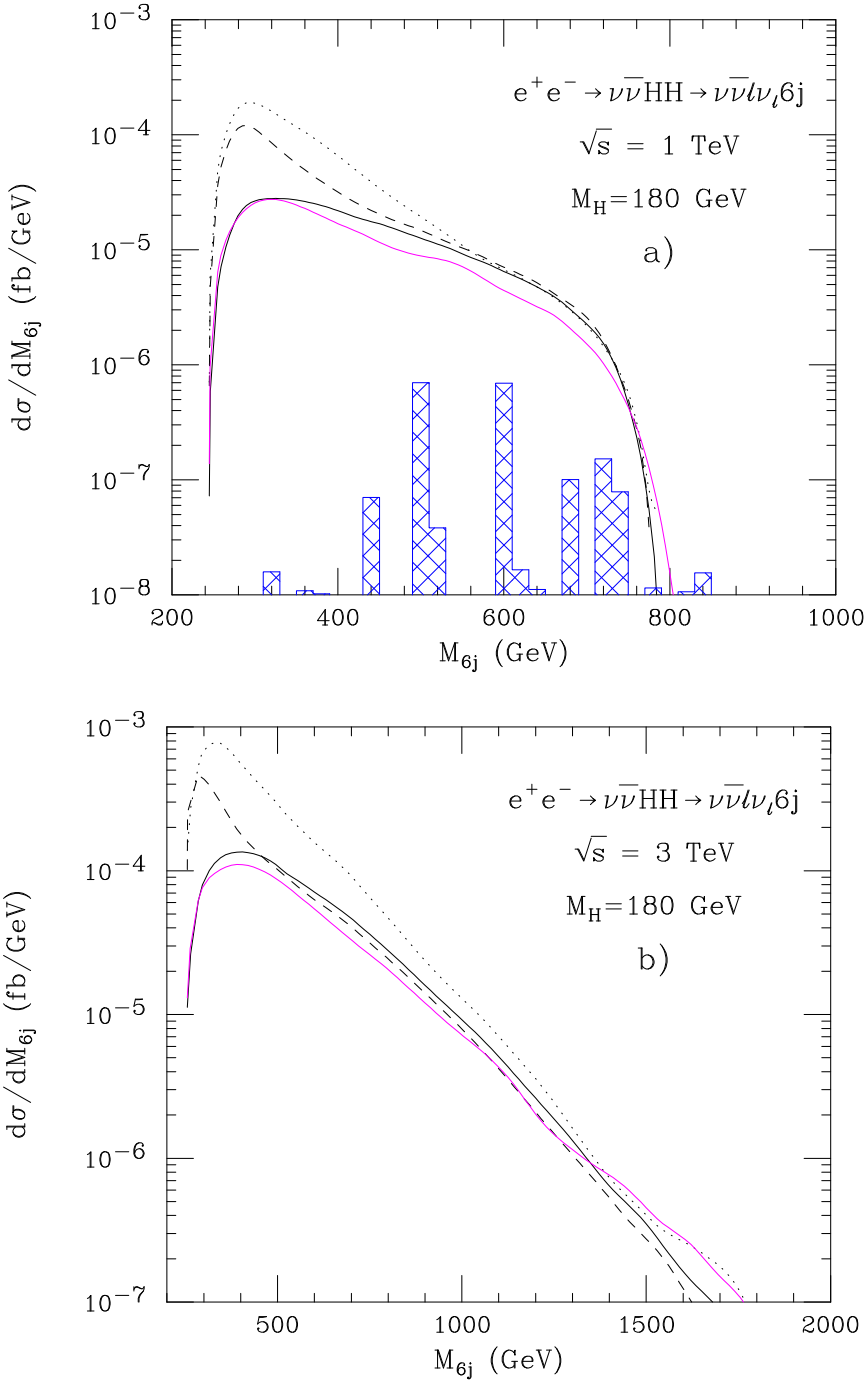

FIG. 11. The $e^+e^- \to \nu\bar{\nu}HH \to \nu\bar{\nu}\ell\nu_\ell 6j$ cross section as a function of the $6j$ invariant mass, M_{6j}, for $m_H = 180$ GeV and a) $\sqrt{s} = 1$ TeV and b) $\sqrt{s} = 3$ TeV. The black solid line is the prediction of the SM signal cross section. The black dashed and dotted lines correspond to the $\nu\bar{\nu}HH$ signal cross section for $\Delta\lambda_{HHH} = +1$ and $\Delta\lambda_{HHH} = -1$, respectively. The magenta line shows the estimated SM cross section for $e^+e^- \to \nu\bar{\nu}\ell\nu_\ell 6j$. The blue hatched histogram in part a) shows the SM $e^+e^- \to W6j$ background. The cuts imposed and the efficiencies used are summarized in Eqs. (6), (8), (10), and (16).

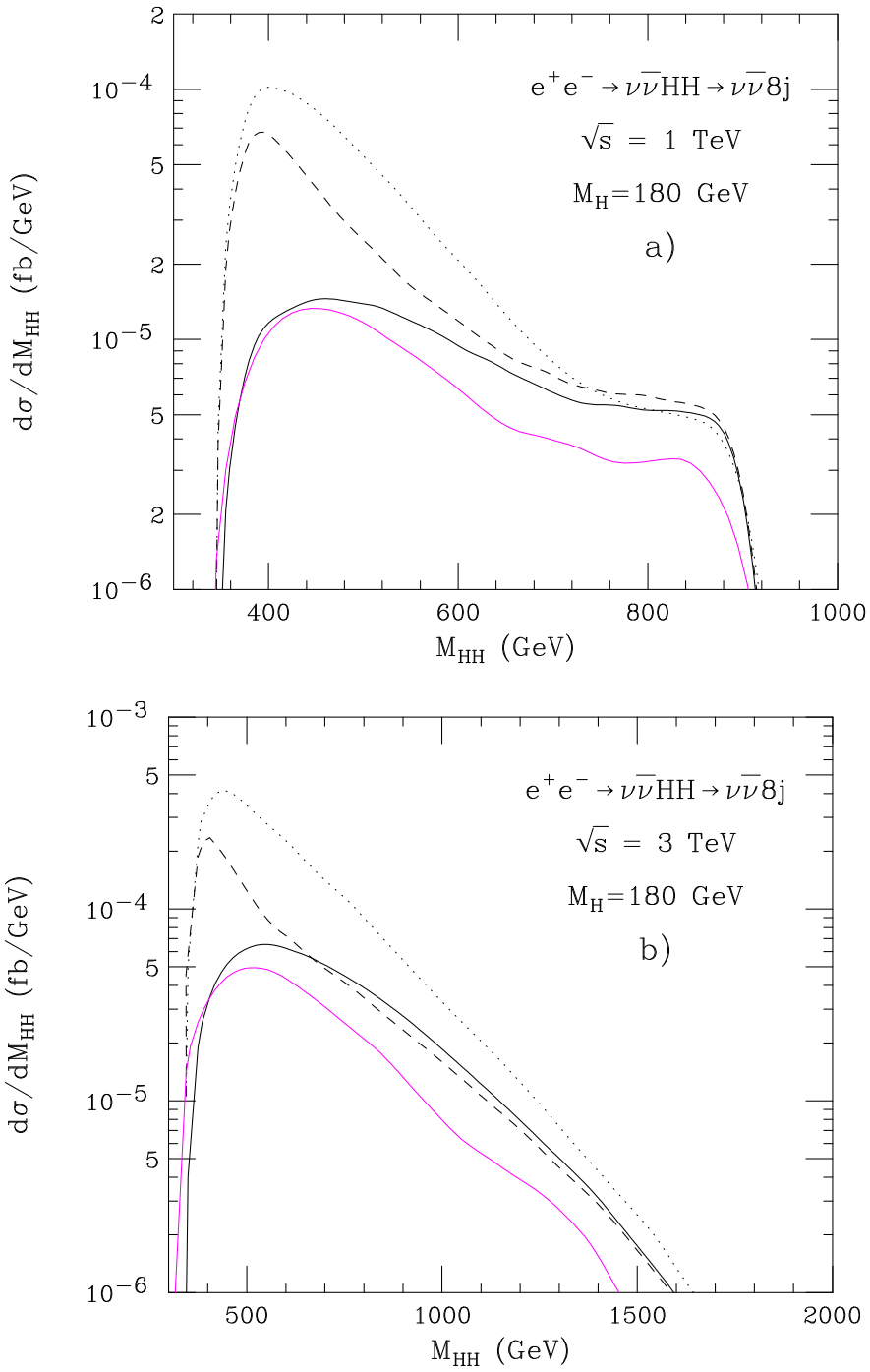

FIG. 12. The $e^+e^- \to \nu\bar{\nu}HH \to \nu\bar{\nu}8j$ cross section as a function of the Higgs pair invariant mass, for $m_H = 180$ GeV and a) $\sqrt{s} = 1$ TeV and b) $\sqrt{s} = 3$ TeV. The black solid line is the prediction of the SM signal cross section. The black dashed and dotted lines correspond to the $\nu\bar{\nu}HH$ signal cross section for $\Delta\lambda_{HHH} = +1$ and $\Delta\lambda_{HHH} = -1$, respectively. The magenta line shows the estimated SM cross section for $e^+e^- \to \nu\bar{\nu}8j$ obtained from the $\nu\bar{\nu}4jH$, $H \to WW \to 4j$ cross section. The cuts imposed and the efficiencies used are summarized in Eqs. (6), (8), (10), and (16).

TABLE II. Cross sections in fb for $e^+e^- \to \nu\bar{\nu}b\bar{b}b\bar{b}$ for $m_H = 120$ GeV and $m_H = 140$ GeV with three or more b-tags, $e^+e^- \to \nu\bar{\nu}4jb\bar{b}$ for $m_H = 140$ GeV, and $e^+e^- \to \nu\bar{\nu}\ell\nu_\ell 6j$ and $e^+e^- \to \nu\bar{\nu}8j$ for $m_H = 180$ GeV. Results are shown for $\sqrt{s} = 1$ TeV and 3 TeV, the SM signal, the full set of Feynman diagrams (labeled "all"), and the reducible backgrounds (labeled "bgd"). The reducible background does not include contributions where the missing transverse momentum originates only from the energy loss of b-quarks and/or jet mismeasurements. The cuts and efficiencies used are listed in Eqs. (6), (8), (10), (11), (15), and (16).

$e^+e^- \to \nu\bar{\nu}b\bar{b}b\bar{b}$			
	signal	all	bgd
$\sqrt{s} = 1$ TeV, $m_H = 120$ GeV	0.026	0.024	0.003
$\sqrt{s} = 1$ TeV, $m_H = 140$ GeV	0.0044	0.0052	0.0014
$\sqrt{s} = 3$ TeV, $m_H = 120$ GeV	0.20	0.16	0.01
$\sqrt{s} = 3$ TeV, $m_H = 140$ GeV	0.040	0.037	0.006
$e^+e^- \to \nu\bar{\nu}4jb\bar{b}$			
	signal	all	bgd
$\sqrt{s} = 1$ TeV, $m_H = 140$ GeV	0.0039	0.0032	–
$\sqrt{s} = 3$ TeV, $m_H = 140$ GeV	0.025	0.023	–
$e^+e^- \to \nu\bar{\nu}\ell\nu_\ell 6j$			
	signal	all	bgd
$\sqrt{s} = 1$ TeV, $m_H = 180$ GeV	0.0065	0.0054	4.0×10^{-5}
$\sqrt{s} = 3$ TeV, $m_H = 180$ GeV	0.050	0.041	$< 1 \times 10^{-6}$
$e^+e^- \to \nu\bar{\nu}8j$			
	signal	all	bgd
$\sqrt{s} = 1$ TeV, $m_H = 180$ GeV	0.0047	0.0036	–
$\sqrt{s} = 3$ TeV, $m_H = 180$ GeV	0.032	0.022	–

largely depends on the resolution of the hadronic calorimeter which can be achieved in an ILC/CLIC experiment.

D. Compilation of cross sections

Before I derive sensitivity limits for the Higgs boson self-coupling, I present, in Table II, integrated signal and background cross sections for $e^+e^- \to \nu\bar{\nu}HH$ and the Higgs boson masses and final states discussed in Secs. V A – V C. Table II shows that, in contrast to ZHH production, the background is always small in $e^+e^- \to \nu\bar{\nu}HH$. Furthermore, the $\nu\bar{\nu}HH \to \nu\bar{\nu}b\bar{b}b\bar{b}$ cross section is considerably larger than that for $ZHH \to jjb\bar{b}b\bar{b}$ for $m_H = 120$ GeV and $m_H = 140$ GeV. Non-resonant diagrams have a moderate effect except for $\nu\bar{\nu}HH \to \nu\bar{\nu}b\bar{b}b\bar{b}$ production and $m_H = 140$ GeV, and for $e^+e^- \to \nu\bar{\nu}8j$. For $\nu\bar{\nu}b\bar{b}b\bar{b}$ production, QCD diagrams contribute at $\mathcal{O}(\alpha_s^2\alpha^4)$. Since these diagrams contribute only $10 - 30\%$ of the cross section over most of the M_{HH} range, I estimate the renormalization scale uncertainty of the $\nu\bar{\nu}HH \to \nu\bar{\nu}b\bar{b}b\bar{b}$ cross section to be no more than 10%.

The main uncertainty of the $e^+e^- \to \nu\bar{\nu}4jb\bar{b}$, $e^+e^- \to \nu\bar{\nu}\ell\nu_\ell 6j$ and $e^+e^- \to \nu\bar{\nu}8j$ cross sections originates from the unknown effect of non-resonant diagrams. Unfortunately, calcu-

lations of these processes including the full set of contributing Feynman diagrams is currently beyond what automated matrix element based programs can handle. I have presented results based on approximations which include subsets of non-resonant diagrams, and argued that these should account for most of the effects of non-resonant diagrams. Nevertheless, an uncertainty of $\mathcal{O}(20\%)$ ($\mathcal{O}(50\%)$) remains for the $e^+e^- \to \nu\bar{\nu}4jb\bar{b}$ and $e^+e^- \to \nu\bar{\nu}\ell\nu_\ell 6j$ ($e^+e^- \to \nu\bar{\nu}8j$) cross section.

VI. SENSITIVITY LIMITS FOR $\Delta\lambda_{HHH}$

I now present quantitative sensitivity limits for the Higgs boson self-coupling for $e^+e^- \to ZHH$ and $e^+e^- \to \nu\bar{\nu}HH$, and the final states discussed in Secs. IV and V. Limits are derived from the M_{HH} distribution except for $e^+e^- \to \nu\bar{\nu}\ell\nu_\ell 6j$ where the $6j$ invariant mass distribution is analyzed. Results are presented for integrated luminosities of 0.5 ab^{-1}, 1 ab^{-1}, and 2 ab^{-1} at $\sqrt{s} = 0.5$ TeV and 1 TeV (ILC), and 1 ab^{-1}, 2 ab^{-1}, and 3 ab^{-1} at $\sqrt{s} = 3$ TeV (CLIC). According to the current ILC (CLIC) design parameters [32,33], an integrated luminosity of 1 ab^{-1} (3 ab^{-1}) corresponds to 5 years of running. For ZHH production, I analyze the $jjb\bar{b}b\bar{b}$ final state with ≥ 3 and 4 b-tags. For $\sqrt{s} = 0.5$ TeV, bounds are calculated for the sets of efficiencies listed in Eqs. (8) and (9), otherwise I only use the efficiencies of Eq. (8). To derive limits, I use the cross sections obtained including non-resonant Feynman diagrams.

As the statistical tool of choice I adopt a log likelihood test. The expression for the log-likelihood function is

$$-2\log L = -2\left[\sum_i \left(-f_S S_i - f_B B_i + n_{0i}\log(f_S S_i + f_B B_i) - \log(n_{0i}!)\right)\right] + \frac{(f_S-1)^2}{(\Delta f_S)^2} + \frac{(f_B-1)^2}{(\Delta f_B)^2}\,. \tag{17}$$

The sum extends over the number of bins, S_i and B_i are the number of signal and background events in the ith bin, and n_{0i} is the number of reference (eg. SM) events in the ith bin. The uncertainties on the signal and background normalizations are taken into account via two multiplicative factors, f_S and f_B, which are allowed to vary but are constrained within the relative uncertainties of the signal and background cross sections, Δf_S and Δf_B, respectively.

In order to simplify the analysis, I assume a common uncertainty for signal and background, $f_S = f_B = f$, in the following. This can be justified by noting that either the signal is considerably larger than the background, or vice versa. In the first case, I use the numerical value of f_S, in the second, f_B is used. The uncertainties, Δf, are determined individually from the renormalization scale uncertainty (if QCD diagrams contribute) or the approximation used to calculate the cross section. These uncertainties have been discussed in Secs. IV and V. In all other cases, a generic theory uncertainty of 10% is assumed to account for unknown higher order electroweak corrections. The values of Δf used in the following analysis are collected in Table III.

The rather large uncertainties listed for $\sqrt{s} = 0.5$ TeV, $m_H = 140$ GeV, and/or ≥ 3 b-tags originate from the large renormalization uncertainty of the (reducible) background and could be reduced by a NLO QCD calculation of $e^+e^- \to b\bar{b}cjjj$ and $e^+e^- \to b\bar{b}c\bar{c}jj$. Such

TABLE III. Theoretical uncertainties, Δf, used in the statistical analysis.

$e^+e^- \to jjb\bar{b}b\bar{b}$, $\epsilon_b = 0.9$, $P_{c\to b} = 0.1$, $P_{j\to b} = 0.005$					
$m_H = 120$ GeV	4 b-tags	≥ 3 b-tags	$m_H = 140$ GeV	4 b-tags	≥ 3 b-tags
$\sqrt{s} = 0.5$ TeV	10%	100%	$\sqrt{s} = 0.5$ TeV	40%	100%
$\sqrt{s} = 1$ TeV	10%	10%	$\sqrt{s} = 1$ TeV	10%	30%
$e^+e^- \to jjb\bar{b}b\bar{b}$, $\epsilon_b = 0.8$, $P_{c\to b} = 0.02$, $P_{j\to b} = 0.001$					
$m_H = 120$ GeV	4 b-tags	≥ 3 b-tags	$m_H = 140$ GeV	4 b-tags	≥ 3 b-tags
$\sqrt{s} = 0.5$ TeV	10%	40%	$\sqrt{s} = 0.5$ TeV	10%	100%
$e^+e^- \to \nu\bar{\nu}b\bar{b}b\bar{b}$					
m_H	$\sqrt{s} = 1$ TeV	$\sqrt{s} = 3$ TeV	m_H	$\sqrt{s} = 1$ TeV	$\sqrt{s} = 3$ TeV
120 GeV	10%	10%	140 GeV	10%	10%

$e^+e^- \to \nu\bar{\nu}4jb\bar{b}$, $m_H = 140$ GeV		$e^+e^- \to \nu\bar{\nu}\ell\nu_\ell 6j$, $m_H = 180$ GeV		$e^+e^- \to \nu\bar{\nu}8j$, $m_H = 180$ GeV	
$\sqrt{s} = 1$ TeV	$\sqrt{s} = 3$ TeV	$\sqrt{s} = 1$ TeV	$\sqrt{s} = 3$ TeV	$\sqrt{s} = 1$ TeV	$\sqrt{s} = 3$ TeV
20%	20%	20%	20%	50%	50%

calculations are beyond the current state of the art of one-loop calculations. Likewise, the uncertainties listed for $e^+e^- \to \nu\bar{\nu}4jb\bar{b}$, $e^+e^- \to \nu\bar{\nu}\ell\nu_\ell 6j$ and $e^+e^- \to \nu\bar{\nu}8j$ could potentially be reduced by performing a full matrix element based tree level calculation of these processes. Further advances in automated tree level programs may make this possible. Alternatively, independent measurements of the relevant cross sections away from the signal region could be used to reduce the theoretical uncertainties.

If $f_S = f_B = f$, $\log L$ can be minimized analytically and one finds the minimum of $\log L$ to occur at

$$f = \frac{1}{2}\left(1 - (\Delta f)^2 N + \sqrt{(1-(\Delta f)^2 N)^2 + 4(\Delta f)^2 N_0}\right), \tag{18}$$

where

$$N = \sum_i (S_i + B_i) \tag{19}$$

is the total number of events,

$$N_0 = \sum_i n_{0i} \tag{20}$$

the total number of reference events, and Δf is the uncertainty of the reference cross section.

The 68.3% confidence level (CL) limits which can be achieved in $e^+e^- \to ZHH \to jjb\bar{b}b\bar{b}$ are listed in Table IV. For a Higgs boson with mass close to the current lower mass bound [1], λ_{HHH} can be measured with a precision of $30-60\%$ in $e^+e^- \to jjb\bar{b}b\bar{b}$ at $\sqrt{s} = 0.5$ TeV with an integrated luminosity of $0.5-2$ ab^{-1}, if one requires 4 b-tags. This result is in qualitative agreement with that reported in Ref. [53]. Since the ZHH cross section falls with increasing center of mass energy, the sensitivities which can be achieved for the same final state and Higgs boson mass at $\sqrt{s} = 1$ TeV are slightly worse. While λ_{HHH} can be measured with reasonable precision in $jjb\bar{b}b\bar{b}$ production for $m_H = 120$ GeV and $\sqrt{s} = 0.5$ TeV, the

TABLE IV. Sensitivities achievable at 68.3% CL for the Higgs boson self-coupling, $\Delta\lambda_{HHH}$ (see Eq. (13)), in $e^+e^- \to ZHH \to jjb\bar{b}b\bar{b}$ for $m_H = 120$ GeV and 140 GeV, $\sqrt{s} = 0.5$ TeV and 1 TeV, and several choices of integrated luminosities. Results are shown for 4 and ≥ 3 b-tags and, for $\sqrt{s} = 0.5$ TeV, two choices of b-tagging efficiencies and misidentification probabilities. I assume the uncertainties listed in Table III. The cuts imposed are described in Secs. III and IV.

$\epsilon_b = 0.9$, $P_{c\to b} = 0.1$, $P_{j\to b} = 0.005$			
	0.5 ab^{-1}	1 ab^{-1}	2 ab^{-1}
$\sqrt{s} = 0.5$ TeV, $m_H = 120$ GeV, 4 b-tags	$^{+0.60}_{-0.56}$	$^{+0.44}_{-0.41}$	$^{+0.33}_{-0.30}$
$\sqrt{s} = 0.5$ TeV, $m_H = 120$ GeV, ≥ 3 b-tags	$^{+1.4}_{-5.2}$	$^{+0.99\quad -3.1}_{-1.12\ ,\ -4.8}$	$^{+0.70\quad -3.5}_{-0.75\ ,\ -4.5}$
$\sqrt{s} = 0.5$ TeV, $m_H = 140$ GeV, 4 b-tags	$^{+2.6}_{-7.7}$	$^{+2.1}_{-6.8}$	$^{+1.7\quad -3.3}_{-2.0\ ,\ -6.0}$
$\sqrt{s} = 0.5$ TeV, $m_H = 140$ GeV, ≥ 3 b-tags	$^{+4.8}_{-8.9}$	$^{+3.6}_{-7.7}$	$^{+2.7}_{-6.9}$
$\sqrt{s} = 1$ TeV, $m_H = 120$ GeV, 4 b-tags	$^{+0.76}_{-0.60}$	$^{+0.53}_{-0.45}$	$^{+0.38}_{-0.33}$
$\sqrt{s} = 1$ TeV, $m_H = 120$ GeV, ≥ 3 b-tags	$^{+0.65}_{-0.58}$	$^{+0.46}_{-0.42}$	$^{+0.33}_{-0.31}$
$\sqrt{s} = 1$ TeV, $m_H = 140$ GeV, 4 b-tags	$^{+1.6}_{-4.2}$	$^{+1.1\quad -2.4}_{-1.0\ ,\ -3.5}$	$^{+0.77}_{-0.71}$
$\sqrt{s} = 1$ TeV, $m_H = 140$ GeV, ≥ 3 b-tags	$^{+1.4}_{-4.1}$	$^{+1.1\quad -2.0}_{-1.1\ ,\ -3.5}$	$^{+0.78}_{-0.77}$
$\epsilon_b = 0.8$, $P_{c\to b} = 0.02$, $P_{j\to b} = 0.001$, ≥ 3 b-tags			
	0.5 ab^{-1}	1 ab^{-1}	2 ab^{-1}
$\sqrt{s} = 0.5$ TeV, $m_H = 120$ GeV	$^{+1.0\quad -4.2}_{-0.8\ ,\ -4.9}$	$^{+0.80}_{-0.65}$	$^{+0.60}_{-0.51}$
$\sqrt{s} = 0.5$ TeV, $m_H = 140$ GeV	$^{+5.1}_{-8.6}$	$^{+3.7}_{-7.3}$	$^{+2.7}_{-6.4}$

significantly reduced signal cross section and the increased background make a measurement of the Higgs boson self-coupling very difficult for $m_H = 140$ GeV in this channel. The sensitivities can be improved somewhat by including other final states such as $HH \to 4jb\bar{b}$, however, the resulting limits are still extremely loose.

The bounds presented here for $m_H = 140$ GeV and $\sqrt{s} = 0.5$ TeV are considerably worse than those derived from the cross section analysis presented in Ref. [26]. This can be traced to the large non-resonant background, and the considerable theoretical uncertainty in the cross section. Both were not taken into account in the earlier analysis.

At a 1 TeV machine, the sensitivity limits which can be achieved in the $jjb\bar{b}b\bar{b}$ final state with 4 b-tags and $m_H = 140$ GeV are approximately a factor 2 less stringent than those found for $m_H = 120$ GeV. Although the signal cross section increases by about a factor 1.5 including the final state with 3 tagged b-quarks, the much increased reducible background, combined with the substantial renormalization uncertainty of the background, ruin the gain from the increased signal cross section for $\sqrt{s} = 0.5$ TeV. For $\sqrt{s} = 1$ TeV, a slight improvement in the sensitivity limits is observed by including the final state with

three tagged b-quarks.

A straightforward technique to reduce the (reducible) background is to choose a b-tagging efficiency somewhat smaller than that of Eq. (8) for which the charm and light quark/gluon mistagging probabilities are lower. Table IV shows that choosing the parameters of Eq. (9) does indeed improve the limits which can be achieved for $\sqrt{s} = 0.5$ TeV and ≥ 3 b-tags, however, the gain is not sufficient to compensate for the increased background and theoretical (renormalization scale) uncertainty which results from including final states with 3 b-tags. Nevertheless, a dedicated search for the b-tagging efficiency and charm and light quark/gluon mistagging probability which optimizes the sensitivity limits for λ_{HHH} may prove beneficial. For a first step in this direction, see Ref. [28]. For $\sqrt{s} = 1$ TeV, the background is always relatively small and not much is gained by varying ϵ_b and the charm and light quark/gluon jet misidentification probabilities.

One of the reasons for the weak sensitivity bounds for ≥ 3 tagged b-quarks is the large renormalization uncertainty of the background cross section. Reducing the renormalization uncertainty requires either the calculation of the NLO QCD corrections for the main background sources, $b\bar{b}cjjj$, $b\bar{b}4j$ and $b\bar{b}c\bar{c}jj$ production, or a precise measurement of the cross section of the processes. It is interesting to investigate how much the sensitivity limits would actually improve if the normalization uncertainty of the background could be reduced to $\Delta f = 10\%$. The sensitivity bounds which one can hope to achieve for $\sqrt{s} = 0.5$ TeV, ≥ 3 tagged b-quarks and the uncertainties listed in Table III, and those obtained for $\Delta f = 10\%$, are compared in Table V. While a reduced theoretical uncertainty will substantially improve the sensitivity limits for ≥ 3 tagged b-quarks, more stringent limits than those found for 4 tagged b-quarks are only found for $m_H = 140$ GeV and the efficiencies of Eq. (9). Of course, further improvements may be possible by optimizing the b-tagging efficiency and charm and light quark/gluon misidentification probabilities. The sensitivity limits which can be achieved for λ_{HHH} in $e^+e^- \to \nu\bar{\nu}HH$ with the theoretical uncertainties of Table III are listed in Table VI. For $m_H = 140$ GeV ($m_H = 180$ GeV), the combined limits from $e^+e^- \to \nu\bar{\nu}b\bar{b}b\bar{b}$ and $e^+e^- \to \nu\bar{\nu}4jb\bar{b}$ ($e^+e^- \to \nu\bar{\nu}\ell\nu_\ell 6j$ and $e^+e^- \to \nu\bar{\nu}8j$) are shown. Since the $b\bar{b}b\bar{b}$ and $b\bar{b}jj$ backgrounds do not affect the M_{HH} differential cross section in the region sensitive to the Higgs boson self-coupling (see Secs. V A and V B), they have not been taken into account in the analysis. The bounds on the Higgs self-coupling which can be achieved in $e^+e^- \to \nu\bar{\nu}HH$ for $m_H = 120$ GeV and 140 GeV at $\sqrt{s} = 1$ TeV are seen to be considerably more stringent than those found for $e^+e^- \to ZHH$ (see Table IV). For $\sqrt{s} = 3$ TeV, λ_{HHH} can be measured with a precision of $10 - 20\%$ for the Higgs boson masses and the integrated luminosities considered here. If the theoretical uncertainty on the cross section for $m_H = 180$ GeV can be reduced to 10%, the bounds listed in Table VI for $\sqrt{s} = 3$ TeV improve by a factor $1.6 - 2$. For $m_H = 140$ GeV ($m_H = 180$ GeV), the sensitivity limits are expected to improve by roughly a factor 1.1 (1.2) if additional final states are included in the analysis.

The bounds derived in this Section should be compared with those one hopes to achieve at the LHC, a luminosity upgraded LHC (SLHC) and a Very Large Hadron Collider (VLHC) [19,20][2]. For the Higgs mass range allowed by current experimental data [1–3],

[2]Ref. [19,20] quotes 95% CL limits. I have recalculated the sensitivity limits for 68.3% CL with

TABLE V. Sensitivities achievable at 68.3% CL for the Higgs boson self-coupling, $\Delta\lambda_{HHH}$ (see Eq. (13)), in $e^+e^- \to ZHH \to jjb\bar{b}b\bar{b}$ with ≥ 3 b-tags for $m_H = 120$ GeV and 140 GeV, $\sqrt{s} = 0.5$ TeV, and several choices of integrated luminosities. Results are shown for the uncertainties listed in Table III and for $\Delta f = 10\%$, and for two choices of b-tagging efficiencies and misidentification probabilities. The cuts imposed are described in Secs. III and IV.

$\epsilon_b = 0.9$, $P_{c\to b} = 0.1$, $P_{j\to b} = 0.005$			
	0.5 ab^{-1}	1 ab^{-1}	2 ab^{-1}
$m_H = 120$ GeV, $\Delta f = 100\%$	$^{+1.4}_{-5.2}$	$^{+0.99}_{-1.12}$, $^{-3.1}_{-4.8}$	$^{+0.70}_{-0.75}$, $^{-3.5}_{-4.5}$
$m_H = 120$ GeV, $\Delta f = 10\%$	$^{+0.86}_{-1.04}$, $^{-4.1}_{-5.1}$	$^{+0.66}_{-0.74}$, $^{-4.2}_{-4.7}$	$^{+0.52}_{-0.56}$
$m_H = 140$ GeV, $\Delta f = 100\%$	$^{+4.8}_{-8.9}$	$^{+3.6}_{-7.7}$	$^{+2.7}_{-6.9}$
$m_H = 140$ GeV, $\Delta f = 10\%$	$^{+3.5}_{-8.0}$	$^{+2.8}_{-7.5}$	$^{+2.3}_{-6.8}$
$\epsilon_b = 0.8$, $P_{c\to b} = 0.02$, $P_{j\to b} = 0.001$			
	0.5 ab^{-1}	1 ab^{-1}	2 ab^{-1}
$m_H = 120$ GeV, $\Delta f = 40\%$	$^{+1.0}_{-0.8}$, $^{-4.2}_{-4.9}$	$^{+0.80}_{-0.65}$	$^{+0.60}_{-0.51}$
$m_H = 120$ GeV, $\Delta f = 10\%$	$^{+0.63}_{-0.63}$	$^{+0.47}_{-0.46}$	$^{+0.36}_{-0.35}$
$m_H = 140$ GeV, $\Delta f = 100\%$	$^{+5.1}_{-8.6}$	$^{+3.7}_{-7.3}$	$^{+2.7}_{-6.4}$
$m_H = 140$ GeV, $\Delta f = 10\%$	$^{+2.5}_{-7.7}$	$^{+1.9}_{-6.9}$	$^{+1.5}_{-6.3}$

the LHC will not be able to probe the Higgs boson self-coupling. At the SLHC, with an integrated luminosity of 6 ab^{-1}, λ_{HHH} can be determined with an accuracy of $50-70\%$ for $m_H = 120$ GeV from $HH \to b\bar{b}\gamma\gamma$, and $10-15\%$ for $m_H = 180$ GeV using the $HH \to 4W \to \ell^\pm\ell'^\pm \not{p}_T 4j$ final state. There are not enough $HH \to b\bar{b}\gamma\gamma$ events for $m_H = 140$ GeV for a viable statistical analysis at the SLHC. A luminosity upgrade of the LHC may be realized at roughly the same time or earlier than an ILC with $\sqrt{s} = 0.5$ TeV. Tables III and IV show that, for $m_H = 120$ GeV, the ILC can measure the Higgs boson self-coupling with considerably higher precision than the SLHC. A measurement of λ_{HHH} for $m_H = 140$ GeV will be very difficult at both machines. For $m_H = 180$ GeV, the SLHC shows a clear advantage, however, a recent combination of electroweak precision data and direct limits from the Tevatron experiments excludes a SM Higgs boson with $m_H = 180$ GeV at more than 2σ [3].

An upgraded ILC with $\sqrt{s} = 1$ TeV considerably improves the chances to determine λ_{HHH} for $m_H = 140$ GeV (see Tables IV and VI). For $m_H = 180$ GeV, however, the SLHC still promises a more precise measurement. Since sensitivity bounds scale roughly like $(\int \mathcal{L}dt)^{(1/4)}$, this statement is true as long as an integrated luminosity larger than 2 ab^{-1}

otherwise unchanged parameters. The 68.3% CL limits are used for the comparison presented here.

TABLE VI. Sensitivities achievable at 68.3% CL for the Higgs boson self-coupling, $\Delta\lambda_{HHH}$ (see Eq. (13)), in $e^+e^- \to \nu\bar{\nu}HH$ for $\sqrt{s} = 1$ TeV and 3 TeV and several choices of integrated luminosities. For $m_H = 120$ GeV, results are shown for the $\nu\bar{\nu}b\bar{b}b\bar{b}$ final state with ≥ 3 tagged b-quarks. For $m_H = 140$ GeV, the combined limits from $e^+e^- \to \nu\bar{\nu}b\bar{b}b\bar{b}$ with ≥ 3 b-tags and $e^+e^- \to \nu\bar{\nu}4jb\bar{b}$ are listed, and for $m_H = 180$ GeV the combined limits from $e^+e^- \to \nu\bar{\nu}\ell\nu_\ell 6j$ and $e^+e^- \to \nu\bar{\nu}8j$ are given. The cuts imposed are described in Secs. III and V. The theoretical uncertainties used are listed in Table III.

$\sqrt{s} = 1$ TeV			
	0.5 ab^{-1}	1 ab^{-1}	2 ab^{-1}
$m_H = 120$ GeV	$^{+0.58}_{-0.27}$	$^{+0.30}_{-0.21}$	$^{+0.20}_{-0.17}$
$m_H = 140$ GeV	$^{+0.99}_{-0.41}$	$^{+0.94}_{-0.38}$	$^{+0.78}_{-0.25}$
$m_H = 180$ GeV	$^{+0.56}_{-0.32}$	$^{+0.55}_{-0.29}$	$^{+0.59}_{-0.28}$
$\sqrt{s} = 3$ TeV			
	1 ab^{-1}	2 ab^{-1}	3 ab^{-1}
$m_H = 120$ GeV	$^{+0.14}_{-0.12}$	$^{+0.11}_{-0.10}$	$^{+0.10}_{-0.09}$
$m_H = 140$ GeV	$^{+0.15}_{-0.19}$	$^{+0.15}_{-0.15}$	$^{+0.11}_{-0.14}$
$m_H = 180$ GeV	$^{+0.16}_{-0.20}$	$^{+0.15}_{-0.13}$	$^{+0.12}_{-0.12}$

can be accumulated at the SLHC.

The results for a 3 TeV e^+e^- collider (CLIC) should be compared with those which one can hope to achieve at a VLHC. Such a machine, assuming a center of mass energy of $\sqrt{s} = 200$ TeV and an integrated luminosity of 600 fb^{-1}, can determine the Higgs boson self-coupling for $m_H = 120$ GeV ($m_H = 140$ GeV) in the $HH \to b\bar{b}\gamma\gamma$ final state with a precision of $30 - 50\%$ ($40 - 60\%$). At CLIC, on the other hand, a precision of $10 - 20\%$ can be achieved for both values of m_H. For $m_H = 180$ GeV, a VLHC can achieve a precision of about 2%. Assuming that a 10% theoretical uncertainty on the cross section can eventually be realized, the sensitivity of a 3 TeV e^+e^- collider obtained from the combined $\nu\bar{\nu}\ell\nu_\ell 6j$ and $\nu\bar{\nu}8j$ final states is limited to $7 - 12\%$. The two final states together account for about 43% of all $HH \to 4W$ decays. Including more $4W$ final states thus is expected to improve these limits by roughly a factor $2^{1/4} \approx 1.2$. A VLHC therefore may yield more precise information on the Higgs boson self-coupling than CLIC for $m_H = 180$ GeV.

VII. SUMMARY AND CONCLUSIONS

After discovery of an elementary Higgs boson at the LHC, and tests of its fermionic and gauge boson couplings, experimental evidence that the shape of the Higgs potential has the form required for electroweak symmetry breaking will complete the proof that both, fermion and weak boson masses, are generated by spontaneous symmetry breaking. To probe the

Higgs potential, one must determine the Higgs boson self-coupling.

Only Higgs boson pair production at colliders can accomplish this. Several years ago, studies have appeared in the literature [18–22], exploring the potential of the LHC, a luminosity upgraded LHC, and a Very Large Hadron Collider to probe the Higgs boson self-coupling. There are also numerous analyses of Higgs boson pair production at e^+e^- colliders [16,17,23–30] which usually only explore one particular Higgs mass and/or final state, or only one center of mass energy. Furthermore, backgrounds are estimated using a leading-log shower approximation, and the effect on non-resonant diagrams is not taken into account.

In this paper, I have presented a more comprehensive analysis of Higgs pair production in e^+e^- collisions. Both ZHH and $\nu\bar{\nu}HH$ production have been investigated for several Higgs boson masses and center of mass energies. The cross section for $\nu\bar{\nu}HH$ production is much smaller than that for ZHH production for $\sqrt{s} = 0.5$ TeV and below. However, it grows quickly with increasing energies, and becomes the dominant source of Higgs boson pairs for $\sqrt{s} \geq 1$ TeV. ZHH ($\nu\bar{\nu}HH$) production therefore was studied for $\sqrt{s} \leq 1$ TeV ($\sqrt{s} \geq 1$ TeV) only. Acceptance cuts and minimal detector effects in form of Gaussian smearing, as well as the energy loss of b-quarks were taken into account in all calculations. The efficiencies and misidentification probabilities used are summarized in Eqs. (8) and (9). The distribution of the Higgs pair invariant mass, M_{HH}, was found to be sensitive to the Higgs boson self-couplings and was used for a log-likelihood based sensitivity analysis.

For ZHH production, I concentrated on the $ZHH \to jjb\bar{b}b\bar{b}$ final state, requiring that the two light quark jets are consistent with a Z-boson. Requiring four tagged b-quarks, the $jjb\bar{b}c\bar{c}$ and $b\bar{b}4j$ backgrounds were found to be relatively small for $m_H = 120$ GeV and $\sqrt{s} = 0.5$ TeV. Non-resonant diagrams change the $jjb\bar{b}b\bar{b}$ cross section by about 10%. For $m_H = 140$ GeV, on the other hand, taking into account the non-resonant diagrams roughly doubles the cross section, while the $jjb\bar{b}c\bar{c}$ background can easily be as large as the signal cross section. This, together with the extremely small signal cross section, and the large renormalization uncertainty of the reducible background cross section, implies that it will be extremely difficult to measure the Higgs boson self-coupling in $jjb\bar{b}b\bar{b}$ production with four tagged b-quarks and $m_H = 140$ GeV at an ILC with a center of mass energy of 0.5 TeV. At $\sqrt{s} = 1$ TeV, the reducible and non-resonant backgrounds are significantly smaller than at a 0.5 TeV collider, and a rough measurement of λ_{HHH} in $e^+e^- \to jjb\bar{b}b\bar{b}$ may be possible for $m_H = 140$ GeV.

To increase the signal cross section, one can include other Z and/or Higgs decay final states. Since $B(Z \to \ell^+\ell^-)$ is small, there will be little gain by including the $\ell^+\ell^-b\bar{b}b\bar{b}$ final state in the analysis. For $m_H = 140$ GeV, $B(H \to WW^* \to 4j) \approx 23\%$. If one of the Higgs bosons in ZHH production decays into four jets, the final state consists of $b\bar{b}6j$. Since the combinatorial background complicates identification of which jets originate from Higgs and which from Z-boson decays, I have not considered $b\bar{b}6j$ production here.

A more straightforward approach is to increase the signal cross section by taking into account final states where only three b-quarks are tagged. Requiring only three tagged b-quarks strongly increases the reducible background and this more than compensates the potential gain in sensitivity from the increased signal cross section. However, the reducible background can be reduced by choosing a different working point in $\epsilon_b - P_{c\to b} - P_{j\to b}$ space. Replacing the efficiencies and misidentification probabilities of Eq. (8) with those of Eq. (9), however, yields only a minor improvement in the sensitivity to λ. Nevertheless, a search for

an optimal working point similar to that in Ref. [28] may be promising.

For $\sqrt{s} = 1$ TeV, the $\nu\bar{\nu}b\bar{b}b\bar{b}$ cross section is about a factor two larger than that for $jjb\bar{b}b\bar{b}$ production. Furthermore, the reducible background is small, both for $m_H = 120$ GeV and 140 GeV. Non-resonant diagrams modify the M_{HH} differential cross section by $\mathcal{O}(10\%)$ except close to the HH threshold where they have a much larger effect. The effect from non-resonant diagrams therefore can be easily confused with a positive anomalous Higgs self-coupling, $\lambda_{HHH} > 0$ (see Figs. 6a and 7a). Due to the larger cross section, and the reduced background, the bounds which can be obtained for $m_H = 120$ GeV are significantly better than those one may hope to achieve in $ZHH \to jjb\bar{b}b\bar{b}$.

For $m_H = 140$ GeV, the signal cross section can be increased by including the $\nu\bar{\nu}b\bar{b}4j$ final state which results when one of the Higgs bosons decays via $H \to WW^* \to 4j$. Combining the limits from $\nu\bar{\nu}b\bar{b}b\bar{b}$ and $\nu\bar{\nu}b\bar{b}4j$ production, I found that the Higgs boson self-coupling can be probed with $25-80\%$ accuracy with 2 ab^{-1} at a 1 TeV e^+e^- collider. Such a machine will also be able to probe λ for a heavier Higgs boson. For $m_H = 180$ GeV, and utilizing the two final states with the largest branching ratios, $HH \to 4W \to \ell^\pm\nu_\ell 6j$ and $HH \to 4W \to 8j$, I found that a 1 TeV e^+e^- collider can probe λ with an accuracy of $30 - 60\%$. A 3 TeV collider will be able to measure the Higgs boson self-coupling with a precision of $10 - 20\%$ for the Higgs boson masses investigated here.

A `MadEvent` based calculation of the full set of non-resonant Feynman diagrams contributing to $\nu\bar{\nu}b\bar{b}4j$, $\nu\bar{\nu}\ell\nu_\ell 6j$ and $\nu\bar{\nu}8j$ production is currently not feasible as it requires very large computing resources. Other programs, which are not based on the evaluation of Feynman diagrams promise a solution for this problem in the future, however, these programs are currently not able to handle the final states of interest. In absence of a calculation which includes the full set of non-resonant Feynman diagrams, I have estimated their effect from calculations which include sub-sets of the non-resonant Feynman diagrams. Unavoidably, this introduces a theoretical uncertainty in the cross section which I have assumed to be of the same size as the effect from those non-resonant diagrams which were included in the calculation. If this uncertainty can be reduced in the future by a calculation which includes the full set of non-resonant Feynman diagrams, the bounds which can be achieved will improve by a factor 1.6 – 2.

Uncertainties in the calculations presented in this paper also originate from the detector performance assumed. A better resolution of the hadronic calorimeter than that assumed such as that promised by the particle flow algorithm [64] may make it possible to tighten the invariant mass window for b-jet and light quark/gluon jet pairs. This would reduce both reducible and irreducible backgrounds and thus improve the sensitivity to anomalous Higgs boson self-couplings. The reducible backgrounds in final states involving b-quarks strongly depend on the charm and light quark/gluon jet misidentification probabilities. More powerful algorithms for tagging b-quarks may well reduce the misidentification probabilities in the future.

One of the main results of the calculations presented here is that a 0.5 TeV ILC will be able to determine the Higgs boson self-coupling only if the Higgs boson mass is rather close to the current lower bound. In contrast, at a 1 TeV e^+e^- linear collider it will be possible to measure λ for larger values of m_H, and to reach a significantly higher precision than for $\sqrt{s} = 0.5$ TeV. The precision which can be reached at a 1 TeV ILC for $m_H \leq 140$ GeV is considerably better than that one can hope to achieve at the SLHC or a VLHC. For a

heavier Higgs boson with $m_H = 180$ GeV, which is disfavored by a global fit to electroweak data and current direct limits, on the other hand, the SLHC and VLHC promise better limits. Even a 3 TeV e^+e^- collider will not be able to measure the Higgs boson self-coupling for $m_H = 180$ GeV more accurately than a VLHC.

ACKNOWLEDGMENTS

I would like to thank J. Reuter for his help with `WHIZARD` and for useful discussions, and F. Krauss for an in-depth discussion on the capabilities of `Sherpa`. I would also like to thank the High Energy Physics Group at Michigan State University, where most of this work was done, for their generous hospitality. This research was supported by the National Science Foundation under grants No. PHY-0456681 and PHY-0757691.

REFERENCES

[1] [ALEPH Collaboration and CDF Collaboration and D0 Collaboration and DELPHI Collaboration and L3 Collaboration and OPAL Collaboration and SLD Collaboration and LEP Electroweak Working Group and Tevatron Electroweak Working Group and SLD Electroweak Working Group and Heavy Flavour Group], arXiv:0811.4682 [hep-ex]; H. Flaecher, M. Goebel, J. Haller, A. Hoecker, K. Moenig and J. Stelzer, Eur. Phys. J. C **60**, 543 (2009) [arXiv:0811.0009 [hep-ph]].

[2] The TEVNPH Working Group, arXiv:0903.4001 [hep-ex].

[3] M. Goebel, arXiv:0905.2488 [hep-ph].

[4] M. Dittmar and H. K. Dreiner, Phys. Rev. D **55**, 167 (1997); D. Rainwater and D. Zeppenfeld, Phys. Rev. D **60**, 113004 (1999) [Erratum-ibid. D **61**, 099901 (2000)]; N. Kauer, T. Plehn, D. Rainwater and D. Zeppenfeld, Phys. Lett. B **503**, 113 (2001); N. Akchurin *et al.*, CMS-NOTE-2002/066; B. Mellado, ATL-CONF-2002-004.

[5] S. Asai *et al.*, ATL-PHYS-2003-005; G. Azuelos and R. Mazini, ATL-PHYS-2003-004; M. Dührssen, ATL-PHYS-2003-010.

[6] ATLAS TDR, report CERN/LHCC/99-15 (1999); G. Aad *et al.* [The ATLAS Collaboration], arXiv:0901.0512.

[7] G. L. Bayatian *et al.* [CMS Collaboration], J. Phys. G **34**, 995 (2007).

[8] D. Rainwater, D. Zeppenfeld and K. Hagiwara, Phys. Rev. D **59**, 014037 (1999); T. Plehn, D. Rainwater and D. Zeppenfeld, Phys. Lett. B **454**, 297 (1999) and Phys. Rev. D **61**, 093005 (2000).

[9] D. Zeppenfeld, R. Kinnunen, A. Nikitenko and E. Richter-Was, Phys. Rev. D **62**, 013009 (2000); M. Hohlfeld, ATL-PHYS-2001-004; M. Dührssen, S. Heinemeyer, H. Logan, D. Rainwater, G. Weiglein and D. Zeppenfeld, Phys. Rev. D **70**, 113009 (2004) [arXiv:hep-ph/0406323]; R. Lafaye, T. Plehn, M. Rauch, D. Zerwas and M. Dührssen, arXiv:0904.3866 [hep-ph].

[10] D. Rainwater, Phys. Lett. B **503**, 320 (2001); V. Drollinger, T. Müller and D. Denegri, arXiv:hep-ph/0201249.

[11] V. Drollinger, T. Müller and D. Denegri, arXiv:hep-ph/0111312; V. Kostioukhine, J. Leveque, A. Rozanov, and J.B. de Vivie, ATL-PHYS-2002-019; D. Green *et al.*, FERMILAB-FN-705 (August 2001); F. Maltoni, D. Rainwater and S. Willenbrock, Phys. Rev. D **66**, 034022 (2002); A. Belyaev and L. Reina, JHEP **0208**, 041 (2002); A. Belyaev, F. Maltoni and L. Reina, in *Proc. of the APS/DPF/DPB Summer Study on the Future of Particle Physics (Snowmass 2001)* ed. N. Graf, arXiv:hep-ph/0110274.

[12] O. J. Éboli and D. Zeppenfeld, Phys. Lett. B **495**, 147 (2000).

[13] T. Plehn and D. Rainwater, Phys. Lett. B **520**, 108 (2001); T. Han and B. McElrath, Phys. Lett. B **528**, 81 (2002).

[14] J. A. Aguilar-Saavedra *et al.* [ECFA/DESY LC Physics Working Group Collaboration], arXiv:hep-ph/0106315 and references therein; T. Abe *et al.* [American Linear Collider Working Group Collaboration], in *Proc. of the APS/DPF/DPB Summer Study on the Future of Particle Physics (Snowmass 2001)* ed. R. Davidson and C. Quigg, arXiv:hep-ex/0106056 and references therein; A. Djouadi *et al.* [ILC Collaboration], arXiv:0709.1893 [hep-ph].

[15] D. A. Dicus, C. Kao and S. S. Willenbrock, Phys. Lett. B **203**, 457 (1988); E. W. N. Glover and J. J. van der Bij, Nucl. Phys. B **309**, 282 (1988); E. W. N. Glover

and J. J. van der Bij, CERN-TH-5022-88, in Proceedings of the *"23rd Rencontres de Moriond: Current Issues in Hadron Physics, Les Arcs, France, Mar 13-19, 1988*; G. Cynolter, E. Lendvai and G. Pocsik, hep-ph/0003008, Acta Phys. Polon. B **31**, 1749 (2000).
[16] F. Boudjema and E. Chopin, Z. Phys. C **73**, 85 (1996).
[17] V. A. Ilyin *et al.*, Phys. Rev. D **54**, 6717 (1996).
[18] F. Gianotti *et al.*, Eur. Phys. J. C **39**, 293 (2005) [arXiv:hep-ph/0204087].
[19] U. Baur, T. Plehn and D. Rainwater, Phys. Rev. Lett. **89**, 151801 (2002) and Phys. Rev. D **67**, 033003 (2003).
[20] U. Baur, T. Plehn and D. Rainwater, Phys. Rev. D **69**, 053004 (2004) [arXiv:hep-ph/0310056].
[21] U. Baur, T. Plehn and D. L. Rainwater, Phys. Rev. D **68**, 033001 (2003) [arXiv:hep-ph/0304015].
[22] A. Blondel, A. Clark and F. Mazzucato, ATL-PHYS-2002-029 (November 2002).
[23] A. Djouadi, W. Kilian, M. Mühlleitner and P. M. Zerwas, Eur. Phys. J. C **10**, 27 (1999).
[24] D. J. Miller and S. Moretti, Eur. Phys. J. C **13**, 459 (2000).
[25] M. Battaglia, E. Boos and W. M. Yao, in *Proc. of the APS/DPF/DPB Summer Study on the Future of Particle Physics (Snowmass 2001)* ed. R. Davidson and C. Quigg, arXiv:hep-ph/0111276.
[26] C. Castanier, P. Gay, P. Lutz and J. Orloff, arXiv:hep-ex/0101028.
[27] Y. Yasui *et al.*, arXiv:hep-ph/0211047.
[28] D. E. Boumediene and P. Gay, *In the Proceedings of 2007 International Linear Collider Workshop (LCWS07 and ILC07), Hamburg, Germany, 30 May - 3 Jun 2007, pp HIG06* [arXiv:0801.0866 [hep-ex]].
[29] Y. Takubo, arXiv:0901.3598 [hep-ph].
[30] M. F. Giannelli, arXiv:0901.4895 [hep-ex].
[31] R. Belusevic and G. Jikia, Phys. Rev. D **70**, 073017 (2004) [arXiv:hep-ph/0403303].
[32] J. Brau *et al.*, "International Linear Collider reference design report. 1: Executive summary. 2: Physics at the ILC. 3: Accelerator. 4: Detectors," SLAC-R-857.
[33] H. Braun *et al.* [CLIC Study Team Collaboration], CERN-OPEN-2008-021, CLIC-NOTE-764.
[34] J. J. Lopez-Villarejo and J. A. M. Vermaseren, arXiv:0812.3750 [hep-ph].
[35] A. Gutierrez-Rodriguez, M. A. Hernandez-Ruiz, O. A. Sampayo, A. Chubykalo and A. Espinoza-Garrido, J. Phys. Soc. Jap. **77**, 094101 (2008) [arXiv:0807.0663 [hep-ph]].
[36] G. Ambrosio *et al.*, Report No. Fermilab-TM-2149 (2001).
[37] B. W. Lee, C. Quigg and H. B. Thacker, Phys. Rev. Lett. **38**, 883 (1977) and Phys. Rev. D **16**, 1519 (1977).
[38] T. Plehn and M. Rauch, Phys. Rev. D **72**, 053008 (2005) [arXiv:hep-ph/0507321].
[39] S. Kanemura *et al.*, Phys. Lett. B **558**, 157 (2003).
[40] W. Hollik and S. Penaranda, Eur. Phys. J. C **23**, 163 (2002); A. Dobado, M. J. Herrero, W. Hollik and S. Penaranda, Phys. Rev. D **66**, 095016 (2002).
[41] D. B. Kaplan and H. Georgi, Phys. Lett. **136B**, 183 (1984); H. Georgi, Phys. Lett. **151B**, 57 (1985).
[42] C. Csaki et al., Phys. Rev. D **68**, 035009 (2003); T. Han, H. E. Logan, B. McElrath and L. T. Wang, Phys. Rev. D **67**, 095004 (2003); C. Dib, R. Rosenfeld and A. Zerwekh,

arXiv:hep-ph/0302068.
[43] V. Barger *et al.* Phys. Rev. D **67**, 115001 (2003).
[44] F. Maltoni and T. Stelzer, JHEP **0302**, 027 (2003) [arXiv:hep-ph/0208156]; J. Alwall *et al.*, JHEP **0709**, 028 (2007) [arXiv:0706.2334 [hep-ph]].
[45] M. L. Mangano, M. Moretti, F. Piccinini, R. Pittau and A. D. Polosa, JHEP **0307**, 001 (2003) [arXiv:hep-ph/0206293].
[46] T. Behnke *et al.* [ILC Collaboration], arXiv:0712.2356 [physics.ins-det].
[47] T. Behnke, S. Bertolucci, R. D. Heuer and R. Settles, DESY-01-011, March 2001.
[48] S. M. Xella-Hansen, M. Wing, D. J. Jackson, N. de Groot, and C.J.S. Damerell, LC-PHSM-2003-061.
[49] U. Baur and L. H. Orr, Phys. Rev. D **76**, 094012 (2007) [arXiv:0707.2066 [hep-ph]].
[50] S. Hillert [LCFI Collaboration], *In the Proceedings of 2005 International Linear Collider Workshop (LCWS 2005), Stanford, California, 18-22 Mar 2005, pp 0313.*
[51] G. Belanger *et al.*, Phys. Lett. B **576**, 152 (2003) [arXiv:hep-ph/0309010]; R. Y. Zhang, W. G. Ma, H. Chen, Y. B. Sun and H. S. Hou, Phys. Lett. B **578**, 349 (2004) [arXiv:hep-ph/0308203].
[52] F. Boudjema *et al.*, *In the Proceedings of 2005 International Linear Collider Workshop (LCWS 2005), Stanford, California, 18-22 Mar 2005, pp 0601* [arXiv:hep-ph/0510184].
[53] T. Barklow, talk given at the *2007 International Linear Collider Workshop (LCWS 2007), DESY, Hamburg, Germany, May 30 – June 3, 2007.*
[54] T. Barklow, talk given at the *2007 ALCPG Workshop, Fermilab, 22-26 October 2007.*
[55] T. Gleisberg *et al.* JHEP **0902**, 007 (2009) [arXiv:0811.4622 [hep-ph]].
[56] F. Krauss, R. Kuhn and G. Soff, JHEP **0202**, 044 (2002) [arXiv:hep-ph/0109036].
[57] F. Krauss, private communication
[58] T. Gleisberg and S. Höche, JHEP **0812**, 039 (2008) [arXiv:0808.3674 [hep-ph]].
[59] C. Duhr, S. Höche and F. Maltoni, JHEP **0608**, 062 (2006) [arXiv:hep-ph/0607057].
[60] W. Kilian, T. Ohl and J. Reuter, arXiv:0708.4233 [hep-ph].
[61] A. Cafarella, C. G. Papadopoulos and M. Worek, arXiv:0710.2427 [hep-ph].
[62] M. Moretti, T. Ohl and J. Reuter, arXiv:hep-ph/0102195.
[63] K. Kolodziej and S. Szczypinski, Nucl. Phys. B **801**, 153 (2008) [arXiv:0803.0887 [hep-ph]]; K. Kolodziej, arXiv:0903.3334 [hep-ph].
[64] S. R. Magill, New J. Phys. **9**, 409 (2007).